THE INCLUSION OF VERTICAL TURBULENT DIFFUSION, MOISTURE AND A TROPOPAUSE IN A NUMERICAL MODEL OF STEADY STATE FRONTS

Daniel Francis Glevy

NAVAL POSTGRADUATE SCHOOL
Monterey, California

THESIS

THE INCLUSION OF VERTICAL TURBULENT DIFFUSION, MOISTURE AND A TROPOPAUSE IN A NUMERICAL MODEL OF STEADY STATE FRONTS

by

Daniel Francis Glevy

March 1975

Thesis Advisor: R. T. Williams

Block #20 continued

boundary value coefficients and various ranges of temperature.

The Inclusion of Vertical Turbulent Diffusion, Moisture and a Tropopause in a Numerical Model of Steady State Fronts

by

Daniel Francis Glevy
Lieutenant Commander, United States Navy
B.S. in Engineering, United States Naval Academy, 1964

Submitted in partial fulfillment of the
requirements for the degree of

MASTER OF SCIENCE IN METEOROLOGY

from the

NAVAL POSTGRADUATE SCHOOL
March 1975

ABSTRACT

The numerical frontogenesis model of Williams [1974] is converted to ℓn p vertical spacing and modified to include a higher upper boundary, tropopause and stratosphere, moisture and variable vertical turbulent diffusion coefficients of momentum and heat. The numerical solutions show more realistic quasi-steady fronts forming within 1-2 days. These solutions are examined and compared over a range of various boundary value coefficients and various ranges of temperature.

TABLE OF CONTENTS

LIST OF TABLES

LIST OF ILLUSTRATIONS

LIST OF SYMBOLS AND ABBREVIATIONS

c_p	Specific heat at constant pressure
cb	Centibars
e	Vapor pressure
e_s	Saturation vapor pressure
f	Coriolis parameter
g	Gravity
km	Kilometers
mb	Millibars
q	Specific humidity
p	Pressure; vertical coordinate
r	Relative humidity
t	Time coordinate
u	East-West component of velocity
v	North-South component of velocity
x,y,z	Space coordinates
A_m	Horizontal turbulent diffusion of momentum
A_θ	Horizontal turbulent diffusion of heat
A_q	Horizontal turbulent diffusion of moisture
C_m	Vertical turbulent diffusion of momentum in numerical solutions
C_θ	Vertical turbulent diffusion of momentum in numerical heat
C_q	Vertical turbulent diffusion of momentum in numerical moisture
H	Depth of atmosphere
H_c	Latent heating due to condensation
K	Degrees Kelvin

K_m	Vertical turbulent diffusion of momentum
K_θ	Vertical turbulent diffusion of heat
K_q	Vertical turbulent diffusion of moisture
L_c	Latent heat of condensation
M_A	Sink or source of moisture due to convection
M_C	Sink or source of moisture due to condensation
P	Precipitation
Q_A	Dry convective adjustment
Q_M	Moist convective adjustment
R	Universal gas constant
RH	Relative humidity
S	$\Delta P/H$, constant used to convert to ℓn p spacing
T	Temperature
$\underline{V}$	Horizontal velocity
Y	North-South distance
ω	Vertical velocity in p-system
ϕ	Geopotential
ψ	Stream function
θ	Potential temperature
$\overline{\theta}_I(p_o)$	Initial reference potential temperature
θ_{SE}	Equivalent potential temperature

ACKNOWLEDGEMENTS

The author wishes to express his appreciation to Dr. Roger Terry Williams for his technical assistance, recommendations, encouragement, patience and for the use of his steady-state frontogenesis model which was modified for the experiments conducted.

Thanks are expressed to Dr. Robert J. Renard, who acted as second reader, for his constructive comments on the manuscript, and to Lt. C. J. Cornelius, USN, for his help in making the computer program more understandable through his written comments and extensive use of comment cards.

The author further wishes to acknowledge the W. R. Church Computer Center at the Naval Postgraduate School on whose computer system IBM 360/67 all computations were performed. Especially helpful was the able and unselfish advice of Mr. David Norman whose expertise in the computer system helped considerably.

A final sincere acknowledgement is given to Linda M. Glevy without whose encouragement, patience and typing this study could not have been completed successfully. And to Pat and Mike Glevy who had to put up with a "bear" for a Daddy for quite awhile.

I. INTRODUCTION

Hoskins and Bretherton [1972] have shown analytically, and Williams [1967, 1972] has shown numerically that discontinuous fronts can form within a finite period of time if no turbulent diffusion is present. These studies suggest that a discontinuity will form within 24 to 36 hours when reasonable initial conditions are used. If turbulent diffusion is present, it can be expected that a balance will be achieved between the frontogenetic advections and turbulent diffusions of momentum, heat, and moisture. The front should remain in this state of quasi-balance as long as the large scale deformation field causes frontogenetic advections around the front.

The numerical frontogenesis model of Williams [1974] shows the effects of horizontal and vertical turbulent diffusions of momentum and heat in the formation of these quasi-steady fronts. This model which includes an Ekman boundary layer will hereafter be referred to as W74 and the model as it existed in Williams [1972] will be referred to as W72. Cornelius [1974] added moisture with its subsequent condensation and release of latent heat to W74. This investigation raises the upper boundary, includes a tropopause and stratosphere and appends variable vertical turbulent momentum and heat diffusion coefficients to the work of Cornelius [1974].

The purpose of this study is to obtain and examine frontal solutions throughout a four-day period. The physical model is essentially the same as one of the models treated by Hoskins [1971] and Hoskins and Bretherton [1972]. The basic model, as it now exists, numerically describes frontogenesis which is forced by a nondivergent horizontal wind field which contains stretching deformation. This deformation wind field is constant in time and independent of height, except in the Ekman boundary layer. The moist hydrostatic primitive equations with diffusion are used in which the time dependent quantities are functions of y and p only. Therefore, output from the model is in the form of vertical cross-sections in the Y-P plane.

The model of W74 has been transformed to pressure coordinates to obtain more accurate values of pressure for the moisture equations of Cornelius [1974].

In Section II, the basic forecast equations are developed and a simplification which keeps the problem two-dimensional is discussed. The initial conditions are presented in Section III. Convective adjustment processes and latent heat release in the model are included in Section IV. The experiments undertaken are examined in Section V and conclusions are given in Section VI.

II. BASIC EQUATIONS AND BOUNDARY CONDITIONS

The hydrostatic primitive equations with diffusion and moisture may be written as follows:

$$\frac{\partial \underline{V}}{\partial t} + \nabla\cdot(\underline{V}\underline{V}) + \frac{\partial(\omega \underline{V})}{\partial p} + \nabla\phi + f(\underline{k}\times\underline{V}) = A_M \nabla^2 \underline{V} + \frac{\partial}{\partial p}\left(K_M \frac{\partial \underline{V}}{\partial p}\right), \tag{2.1}$$

$$\frac{\partial \theta}{\partial t} + \nabla\cdot(\theta \underline{V}) + \frac{\partial}{\partial p}(\omega\theta) = A_\theta \nabla^2 \theta + \frac{\partial}{\partial p}\left(K_\theta \frac{\partial \theta}{\partial p}\right) + Q_A + Q_M + H_c, \tag{2.2}$$

$$\frac{\partial q}{\partial t} + \nabla\cdot(q\underline{V}) + \frac{\partial}{\partial p}(\omega q) = A_q \nabla^2 q + \frac{\partial}{\partial p}\left(K_q \frac{\partial q}{\partial p}\right) + M_A - M_C, \tag{2.3}$$

$$\nabla\cdot\underline{V} + \frac{\partial \omega}{\partial p} = 0, \tag{2.4}$$

$$\frac{\partial \phi}{\partial p} = -L(p), \tag{2.5}$$

where

$$L(p) = \frac{R}{p}\left(\frac{p}{p_o}\right)^\kappa = c_p \frac{\partial}{\partial p}\left(\frac{p}{p_o}\right)^\kappa.$$

The equations are in pressure coordinates with slight modification due to the addition of the equation of conservation of water vapor (2.3) which is analogous to the thermodynamic equation (2.2). Sinks and sources of heat and moisture have been added to the thermodynamic equation (2.2) and the conservation of water vapor equation (2.3).

The quantities, A_M, A_θ and A_q are the horizontal turbulent diffusion coefficients of momentum, heat and moisture, respectively, while K_M, K_θ and K_q are the corresponding vertical coefficients. These coefficients were assigned various reasonable values in the following experiments. Dry and moist convective adjustment processes are represented by the functions Q_A and Q_M while latent heating due to large scale condensation is represented by H_c. The quantity M_A is a sink or source of moisture due to moist convective adjustment in the moisture equation, while M_C is a sink for moisture due to large scale condensation.

Boundary conditions for the above equations are such that the domain has a flat lower boundary and a constant pressure surface where $\omega = 0$ as the upper boundary. The no slip condition is used at the lower boundary and the no stress condition is used at the upper boundary. The conditions are as follows:

$$\omega(x,y,0,t) = \omega(x,y,p_t,t) = 0$$

$$\underline{V}(x,y,0,t) = 0$$

$$K_M \frac{\partial \underline{V}}{\partial p}(x,y,p_t,t) = 0 \qquad (2.6)$$

$$K_\theta \frac{\partial \theta}{\partial p}(x,y,0,t) = K_\theta \frac{\partial \theta}{\partial p}(x,y,p_t,t) = 0$$

$$K_q \frac{\partial q}{\partial p}(x,y,0,t) = K_q \frac{\partial q}{\partial p}(x,y,p_t,t) = 0$$

where p_t represents the pressure level at the top of the domain, and 0 corresponds to p_o at the bottom.

The approximate steady-state solutions to the hydrostatic primitive equations [(2.1) - (2.5)] are:

$$\underline{V} = \underline{U} = D\,[x(1-e^{-\zeta}\cos\zeta) + ye^{-\zeta}\sin\zeta]\underline{i} - y(1-e^{-\zeta}\cos\zeta) - xe^{-\zeta}\sin\zeta)\underline{j}, \qquad (2.7)$$

$$\omega = 0,$$

$$\phi = \Phi \equiv -D^2(x^2+y^2)/2 - fDxy + F(p),$$

$$\theta = G(p),$$

$$q = H(p),$$

where

$\zeta = \left(\frac{f}{2K_M}\right)^{\frac{1}{2}}(p_o - p)$, K_M is evaluated at p_o, D and f are constants and where F(p) is such that the hydrostatic equation (2.5) is satisfied. The functions G(p) and H(p) are arbitrary functions of p since $\omega = 0$. These solutions satisfy the boundary conditions (2.6) and allow for inclusion of the Ekman boundary layer. The relations (2.7) satisfy the steady-state equations if some small advection terms in the boundary layer are neglected as they usually are in Ekman theory.

The equations and the model become two-dimensional as in W74 and Cornelius [1974] after a subdivision of dependent variables as follows:

$$\begin{aligned} \underline{V} &= \underline{U}(x,y,p) + u(y,p,t)\underline{i} + v(y,p,t)\underline{j} \\ \omega &= \omega(y,p,t) \\ \theta &= \theta(y,p,t) \\ \phi &= \Phi(x,y) + \pi(y,p,t) \\ q &= q(y,p,t) \end{aligned} \qquad (2.8)$$

It is noted that all departures from the approximate steady deformation solutions (2.7) are assumed to be independent of x. If we substitute the relations (2.8) in the component of (2.1) we obtain:

$$\frac{\partial u}{\partial t} + \frac{\partial}{\partial y}(uv) + \frac{\partial}{\partial p}(\omega u) + uD(1-e^{-\zeta}\cos\zeta) - D[y(1-e^{-\zeta}\cos\zeta) - xe^{-\zeta}\sin\zeta]\frac{\partial u}{\partial y} + vDe^{-\zeta}\sin\zeta + \omega D\frac{\partial}{\partial p}[xe^{-\zeta}(1-\cos\zeta) + ye^{-\zeta}\sin\zeta] = fv + A_M\frac{\partial^2 u}{\partial y^2} + \frac{\partial}{\partial p}\left(K_M\frac{\partial u}{\partial p}\right). \quad (2.9)$$

In this study we will neglect the terms in (2.9) where x appears and apply this and the other equations at $x = 0$. If the initial u, v, w, θ, π and q fields are independent of x, the error from this approximation will grow slowly and will be confined to the boundary layer since the x dependent terms of (2.9) are zero outside the boundary layer. Since frontogenesis occurs very rapidly, it is expected that the development of x-variations in the dependent variables would have only a small effect on the resulting quasi-steady front.

In any case these effects could not be observed in the atmosphere, because variations in the basic fields along atmospheric fronts would be much more important.

When equation (2.9) is evaluated at $x = 0$ it becomes

$$\frac{\partial u}{\partial t} + \frac{\partial}{\partial y}(uv) + \frac{\partial}{\partial p}(\omega u) - \Gamma u\frac{\partial V}{\partial y} + \Gamma V\frac{\partial u}{\partial y} - v\frac{\partial V}{\partial y}(e^{-\zeta}\sin\zeta) - V\frac{\partial}{\partial p}(e^{-\zeta}\sin\zeta) = fv + A_M\frac{\partial^2 u}{\partial y^2} + \frac{\partial}{\partial p}\left(K_M\frac{\partial u}{\partial p}\right), \quad (2.10)$$

where $V = -Dy$ and $\Gamma = 1-e^{-\zeta}\cos\zeta$. The $\underline{j}$ component of (2.1) applied at $x = 0$ takes the form

$$\frac{\partial v}{\partial t} + \frac{\partial}{\partial y}(vv) + \frac{\partial}{\partial p}(\omega v) + \Gamma \frac{\partial}{\partial y}(vV) - u \frac{\partial V}{\partial y} e^{-\zeta} \sin \zeta$$

$$- (\omega V) \frac{\partial}{\partial p}(e^{-\zeta} \cos \zeta) = - \frac{\partial \pi}{\partial y} - fu + A_M \frac{\partial^2 u}{\partial y^2} + \frac{\partial}{\partial p}$$

$$(K_M \frac{\partial V}{\partial p}) \quad . \tag{2.11}$$

Similarly the following equation for the departure of potential temperature can be derived from (2.2):

$$\frac{\partial \theta}{\partial t} + \frac{\partial}{\partial y}(v\theta) + \frac{\partial}{\partial p}(\omega\theta) + \Gamma V \frac{\partial \theta}{\partial y} = A_\theta \frac{\partial^2 \theta}{\partial y^2} + \frac{\partial}{\partial p}(K_\theta \frac{\partial \theta}{\partial p})$$

$$+ Q_A + Q_M + H_c \tag{2.12}$$

and the following equation for q from (2.3)

$$\frac{\partial q}{\partial t} + \frac{\partial}{\partial y}(vq) + \frac{\partial}{\partial p}(\omega q) + \Gamma V \frac{\partial q}{\partial y} = A_q \frac{\partial^2 q}{\partial y^2} + \frac{\partial}{\partial p}(K_M \frac{\partial q}{\partial p})$$

$$+ M_A - M_C. \tag{2.13}$$

Equations (2.4) and (2.5) become

$$\frac{\partial v}{\partial y} + \frac{\partial}{\partial p} = 0, \tag{2.14}$$

and

$$\frac{\partial \pi}{\partial p} = -L(p)\theta. \tag{2.15}$$

The boundary conditions at the bottom and top of the domain, respectively, are

$$\begin{aligned} u = v = \omega = K_\theta \frac{\partial \theta}{\partial p} = K_q \frac{\partial q}{\partial p} = 0 \qquad p = p_o \\ K_M \frac{\partial u}{\partial p} = K_M \frac{\partial v}{\partial p} = \omega = K_\theta \frac{\partial \theta}{\partial p} = K_q \frac{\partial q}{\partial p} = 0 \qquad p = p_{top} \end{aligned} \tag{2.16}$$

If we define the vertical average of a quantity as

$$< ( ) > = \frac{1}{p_o - p_{top}} \int_{p_{top}}^{p_o} ( )(dp), \tag{2.17}$$

integrate the hydrostatic equation (2.15) with respect to p and remove the vertical mean, it follows that

$$\pi - < \pi > = [\int_{p_{top}}^{p} L(p)\theta dp - < \int_{p_{top}}^{p_o} L(p)\theta dp >]. \tag{2.18}$$

Taking the vertical average of (2.14) and using the boundary (2.16) gives

$$\frac{\partial}{\partial y} < v > = 0. \tag{2.19}$$

This equation states that the total mass flux in the y-direction is independent of y. In W72 a symmetry argument was used to show that this flux must be zero. This argument does not hold strictly in this experiment, but it can be expected that at large distances from the frontal zone, the disturbance mass flux will vanish. Thus it is assumed that

$$< v > = 0. \tag{2.20}$$

Equation (2.11) can be written

$$\frac{\partial v}{\partial t} + \frac{\partial}{\partial y} [vv - <vv>] + \frac{\partial}{\partial p}(\omega v) + \frac{\partial}{\partial y} (\Gamma vV - <\Gamma v>V)$$
$$- \frac{\partial V}{\partial y} [ue^{-\zeta} \sin \zeta - <ue^{-\zeta} \sin \zeta> - V[\omega \frac{\partial}{\partial p} (e^{-\zeta} \cos \zeta)$$
$$- <\omega \frac{\partial}{\partial p} (e^{-\zeta} \cos \zeta)>] = \frac{\partial}{\partial y} (\pi - <\pi>) - f(u - <u>) + A_M \frac{\partial^2 V}{\partial y^2}$$
$$+ \frac{\partial}{\partial p} (K_M \frac{\partial V}{\partial p}) - \frac{K_M}{p_t} (\frac{\partial V}{\partial p})_{p=p_o}. \tag{2.21}$$

The equations (2.10), (2.12), (2.13), (2.14), (2.18) and (2.20) form a complete set which can be solved by a pure

marching process. The finite difference equations conserve mean squares in the advection terms and are described by Williams [1967]. The Matsuno scheme is used everywhere except in the arrangement of variables and the finite difference approximations are the same as those used by Williams [1967]. In order to close the problem, computational boundaries must be introduced in y. Since the disturbance velocities should die out at a sufficient distance from the axis of dilation, then

$$v(\pm y,p,t) = 0. \tag{2.22}$$

However, there is appreciable inflow across these computational boundaries since $V(\pm Y) = \pm DY$. The quantities u, θ and q which are advected across the boundaries must be specified independent of the interior values if computational stability is to be maintained (Platzman, 1954). Thus, the following boundary conditions are used:

$$\begin{aligned} u[\pm(Y + \Delta y/2), p,t] &= u[\pm(Y + \Delta y/2),p,0] \\ \theta[\pm(Y + \Delta y/2), p,t] &= \theta[\pm(Y + \Delta y/2),p,0] \\ \theta[\pm(Y - \Delta y/2), p,t] &= \theta[\pm(Y - \Delta y/2),p,0] \\ q[\pm(Y + \Delta y/2), p,t] &= q[\pm(Y + \Delta y/2),p,0]. \end{aligned} \tag{2.23}$$

The computational boundaries $y = \pm Y$ are placed between gridpoints so that the above conditions are actually applied at $y = \pm(Y + \Delta y/2)$.

The boundary conditions were found to be satisfactory except that a solution separation developed near the boundaries. This was controlled by using a Matsuno time differencing scheme for stability and because of its damping

characteristics. The vertical gridpoints were spaced proportional to ℓn p using the relation $p = p_o - p_o e^{-sk}$, where s is $\Delta p/H$. Refer to Table II for forecast levels.

III. INITIAL CONDITIONS

The initial conditions of Cornelius [1974] were modified by raising the upper boundary to approximately the 100-mb level, and by simulating a "tropopause" centered at about the 250-mb level. The Cornelius [1974] initial conditions are developed as follows. The initial potential temperature field in pressure coordinates is given by

$$\theta(y,p,0) = \bar{\theta}_I(p_o) \exp\left[\frac{c_p}{g}\frac{\partial\bar{\theta}_I}{\partial z}\left(1 - \left(\frac{p}{p_o}\right)^{\kappa}\right)\right] - a(2/\pi)\arctan(\sinh \alpha y) \qquad (3.1)$$

where

$$\alpha = \frac{f\pi}{H\sqrt{L(p_M)(-\partial\bar{\theta}_I/\partial p)}} = \frac{f\pi}{H\sqrt{(R/p_M)(p/p_M)^{\kappa}(-\partial\bar{\theta}_I/\partial p)_{p_M}}} \qquad (3.2)$$

In the model, α is given a constant median value by solving (3.2) at $p = p_M$ and using the static stability $\partial\theta_I/\partial p$ at this level.

The initial u component of the velocity is found using a form of the hydrostatic equation (2.26) and the definition of geostrophic wind

$$u = -\frac{1}{f}\frac{\partial\phi}{\partial y} . \qquad (3.3)$$

A form of the thermal wind equation is found to be

$$\frac{\partial u}{\partial p} = -\frac{1}{f}\frac{\partial}{\partial y}\frac{\partial\phi}{\partial p} = \frac{1}{f}\frac{R}{p}\left(\frac{p}{p_o}\right)^{\kappa}\frac{\partial\theta}{\partial y} . \qquad (3.4)$$

We again assume a median pressure level p_M where $u(p_M) = 0$, and integrate

$$\int_{p_M}^{p} \frac{\partial u}{\partial p}\, dp = \frac{R}{f} \frac{\partial \theta}{\partial y} \int_{p_M}^{p} \frac{1}{p} \left(\frac{p}{p_o} \right)^{\kappa} dp \qquad (3.5)$$

to get

$$u(y,p,0) = \frac{c_p}{f} \frac{\partial \theta}{\partial y} \left[\left(\frac{p}{p_o} \right)^{\kappa} - \left(\frac{p_M}{p_o} \right)^{\kappa} \right] \qquad (3.6)$$

where

$$\kappa = R/c_p .$$

From equation (4.3), in Williams [1972], it is seen that

$$\frac{\partial \theta}{\partial y} = - \frac{2a\alpha}{\pi} \operatorname{sech} (\alpha y). \qquad (3.7)$$

Therefore, the initial u field is given by

$$u(y,p,0) = - \frac{c_p}{f} \frac{2a\alpha}{\pi} \left[\left(\frac{p}{p_o} \right)^{\kappa} - \left(\frac{p_M}{p_o} \right)^{\kappa} \right] \operatorname{sech} (\alpha y). \qquad (3.8)$$

The initial divergent wind is determined as in Williams [1972] by using the quasi-geostrophic equation in pressure coordinates. The stream function is defined as

$$v = \partial \psi / \partial p$$

and (3.9)

$$\omega = - \partial \psi / \partial y$$

and equation (4.10) in Williams [1972] takes the form

$$- \frac{\partial^2 \psi}{\partial p^2} + L(p_M) \left(- \frac{\partial \theta_I}{\partial p} \right)_{p_M} \frac{\partial^2 \psi}{\partial y} = \frac{2D}{f^2} L(p_M) \frac{\partial \theta}{\partial y} , \qquad (3.10)$$

recalling that

$$L(p_M) = \frac{R}{p_M} \left(\frac{p_M}{p_o} \right)^{\kappa} .$$

The equation (3.10) is solved for ψ from the initial temperature field (3.1) with the technique of Ogura and Charney [1962] and ψ is then determined from (3.9).

These initial conditions do not satisfy the boundary conditions on u, v and θ at the upper and lower boundaries. Hence a period of adjustment will be required to form the surface friction layer and some oscillations may be observed later. The fields of ω and π are obtained through the continuity and hydrostatic equations (2.14) and (2.15).

The initial field of specific humidity is calculated by first determining saturation vapor pressure e_s at each gridpoint through use of an integrated form of the Clausius-Clapeyron equation. According to Hess [1959]

$$e_s = .611 \exp \left(\frac{L_c}{R_v} \left(\frac{1}{T_o} - \frac{1}{T} \right) \right) \tag{3.11}$$

where L_c is the latent heat of condensation, R_v is the gas constant for water vapor, and T_o is a constant of integration. With knowledge of the saturation vapor pressure, the saturation specific humidity is obtained from the approximate relation of Haltiner and Martin [1957]

$$q_s = \frac{.622\ e_s}{p} . \tag{3.12}$$

Knowledge of potential temperature at t = 0 from equation (3.1), makes it possible to calculate q_s at each point using equations (3.11) and (3.12). Defining q to be a given fraction of q_s allows the testing of atmospheres of different constant initial relative humidity. The initial conditions of Cornelius [1974] were modified as follows. A tropopause was simulated centered at about the 250-mb level. This was accomplished using a reference temperature at the midpoint of the horizontal scale and calculating temperatures such

that a tropopause with its expected variation in height was determined and a zero vertical temperature gradient was achieved in the lower stratosphere. The tropopause height varied from 325 to 110 mb over the horizontal domain for $\overline{\theta}_I(p_o) = 290$ K. The tropopause was simulated as follows. A reference temperature was computed using equation (3.1) as

$$T_{ref} = 215 + a \left(\frac{2}{\pi} \right) \arctan(\sinh \alpha y) \left(\frac{p_o - p_{ref}}{p_o} \right)^{\kappa} \quad (3.13)$$

When the temperature in each column reached this reference temperature, it was held constant at that value, as expected in the lower stratosphere. Temperature was then converted back to potential temperature.

IV. CONVECTIVE ADJUSTMENT, LATENT HEAT AND PRECIPITATION

Two additional heating terms (Q_m and H_c) were included in the moist thermodynamic equation (2.2) necessitating further amendment to W74. Atmospheric heating by the dry convective adjustment, Q_a, was included in W74 to eliminate any intense grid scale convection which developed due to the formation of any dry unstable lapse rates. This redistribution of heating was accomplished using averaging techniques to ensure that the dry adiabatic lapse rate was not exceeded ($\partial\theta/\partial p \leq 0$).

Lapse rates were tested in each vertical column of the model as in Cornelius [1974]. Upon encountering an unstable layer ($\partial\theta/\partial p > 0$), a cumulative average was taken and applied to the gridpoints within this layer until neutral stability ($\partial\theta/\partial p = 0$) was attained. The model was checked simultaneously for instabilities developing below the convectively adjusted layer and potential temperatures at these levels were also cumulatively averaged and reassigned the new values. The final result of the technique is that the heating is redistributed to simulate physical processes of the atmosphere and mathematically that $\partial\theta/\partial p \leq 0$ throughout each column of the model. A completely analogous scheme was used for saturated parcels in the moist experiment, only using equivalent potential temperatures, θ_{SE}, in place of potential temperature θ.

The addition of moisture required that large scale condensation and the subsequent release of latent heat be given important consideration. Following Haltiner [1971], changes in moisture and temperature due to large scale condensation were determined as follows.

Where relative humidity exceeds 100%, the adjustments in temperature δT and specific humidity δq are determined by the following equations:

$$q + \delta q = q_s(T + \delta T, p) \tag{4.1}$$

and

$$c_p \delta T = - L_c \delta q. \tag{4.2}$$

These equations require that the final state of the air be exactly saturated and that excess moisture be condensed isobarically, releasing the latent heat to the air.

Equations (4.1) and (4.2) can be expressed in iterative form as

$$\Delta q = q_s(1 - r) + \left(\frac{\partial q_s}{\partial T} \right)_p \Delta T, \quad q = rq_s \tag{4.3}$$

and

$$c_p \Delta T = -L \Delta q. \tag{4.4}$$

Eliminating ΔT from (4.3) and (4.4) gives

$$\Delta q = \frac{q_s(1 - r)}{1 + \frac{L}{c_p} \left(\frac{\partial q_s}{\partial T} \right)}. \tag{4.5}$$

At constant pressure the Clausius-Clapeyron equation can be expressed as

$$\left(\frac{\partial q_s}{\partial T} \right)_p = \frac{L_c}{R_v} \frac{q_s}{T^2}. \tag{4.6}$$

Substituting (4.6) into (4.5) gives

$$\Delta q = \frac{q_s(1 - r)}{1 + c_p \frac{L^2 q_s}{R_v T^2}} \quad . \tag{4.7}$$

Δq may be now calculated from (4.7) as can the corresponding value of ΔT from (4.4). The first estimates of the adjusted temperature and specific humidity are,

$$T' = T + \Delta T \quad \text{and} \quad q' = q + \Delta q. \tag{4.8}$$

These values in turn are used to obtain improved approximations. Iterations are continued until the values of T' and q' at each level match with sufficient accuracy 100% relative humidity. The changes are then applied to the potential temperature and specific humidity fields of the model accounting for the term H_c of equation (2.2) and M_c of equation (2.3).

The model is then investigated for unstable moist convection and its associated heat of condensation. A convective adjustment scheme similar to the dry one is used on the saturated parcels so that moist static stability is always maintained. A field of equivalent potential temperature is formulated according to Holton [1972] as

$$\Theta_{SE} = \Theta \exp \left(\frac{L_c q_s}{c_p T} \right) \tag{4.9}$$

and the moist convective adjustment is designed to ensure that the moist adiabatic lapse rate is not exceeded ($\partial \Theta_{SE} / \partial p \leq 0$).

The heat release, Q_m, as a result of moist convective adjustment is included through knowledge of the change of equivalent potential temperature during the adjustment.

Taking the natural logarithm of both sides of equation (4.9) gives

$$\ell n\ \Theta_{SE} = \ell n\ \Theta\ \frac{L_c q_s}{c_p T} . \tag{4.10}$$

A constant pressure surface may be assumed since the model uses pressure coordinates. Differentiating both sides of (4.10) and recalling the definition of potential temperature gives

$$\frac{d\Theta_{SE}}{\Theta_{SE}} = \frac{dT}{T} + \frac{dq_s\ L_c}{c_p T} - \frac{L_c\ q_s\ dT}{T^2} . \tag{4.11}$$

Solving equation (4.6) for dq_s, substituting into equation (4.11) and solving for dT leads to

$$dT = \frac{d\Theta_{SE}}{\Theta_{SE}\ \frac{1}{T}[(1 + \frac{q_s\ L_c^2}{R_v c_p T^2} - \frac{L\ q_s}{c_p T}\ ]} \tag{4.12}$$

where $d\Theta_{SE}$ is the change in Θ_{SE} needed to adjust ($\partial\Theta_{SE}/\partial p = 0$).

Since the atmosphere remains saturated throughout the process of moist convective adjustment, the Clausius-Clapeyron equation is again used to obtain the corresponding dq or actually dq_s. Changes are again applied to the potential temperature and specific humidity fields of the model accounting for the terms Q_M of equation (2.2) and M_c of equation (2.3).

A cumulative amount of precipitation is then found using the relation

$$P = -\frac{1}{g}\int_{o}^{p_o} \delta q dp \qquad (4.13)$$

in agreement with the changes in specific humidity due to condensation and moist convective adjustment. Precipitation is expressed in inches of rainfall in the model.

V. NUMERICAL SOLUTIONS

All numerical results to be shown use the following values for the constants:

$\Delta t = 540$ sec $\quad p_o = 100$ cb $\quad p_M = 55$ cb

$\Delta p/H = .01978$ $\quad Y = 1800$ KM $\quad \Delta y = 60$ KM

$g = 9.81$ m sec^{-2} $\quad f = 10^{-4}$ sec^{-1} $\quad D = 10^{-1}$ sec^{-1}

$\Theta_o = 300$ K $\quad \theta_I(p_o) = 280, 290, 300$ K $\quad c_p = 1003$ joules Kg^{-1} K^{-1}

$R_v = 461$ joules Kg^{-1} K^{-1} $\quad R = 287$ joules Kg^{-1} K^{-1}

$\kappa = R/c_p$ $\quad L_c = 2.5 \times 10^6$ joules Kg^{-1}

$a = 12.56$ K $\quad RH = 70\%$

$\frac{\partial \theta_I}{\partial z} = 5$ K Km^{-1} $\quad (\frac{\partial \theta_I}{\partial p})_{p_M} = -.53448$ K cb^{-1}

$A_m = A_o = 3 \times 10^4$ m^{2}sec^{-1} $\quad A_q = 100000$ m^{2}sec^{-1}

$C_q = 0$, cb^{2}sec^{-1} $\quad C_{mB} = 0, .001409, .0007$ cb^{2}sec^{-1}

(which corresponds to 0, 10, 5 m^{2}sec^{-1} in height coordinates)

$C_{\theta B} = 0, .0007, .0001761$ cb^{2}sec^{-1} (which corresponds to 0, 5, 1.25 m^{2}sec^{-1} in height coordinates)

where more than one value means that the constant was varied in different experiments. Whenever possible, the values are the same as those used in W74.

The values of vertical diffusion of moisture C_m and heat C_θ were varied in the experiments to compensate for density variation in the atmosphere. This is equivalent to a constant coefficient in the z coordinate system and is accomplished using the following formulae:

$$C_m = C_{mB}(1 - p/p_o)^2 \tag{5.1}$$

and

$$C_\theta = C_{\theta B}(1 - p/p_o)^2 \tag{5.2}$$

in this section numerical frontogenesis solutions with moisture, friction and a stratosphere are examined at t = 4 days and compared to the corresponding dry atmosphere.

As can be seen from Table I, 11 experiments were performed. Experiments 1 and 2 contain only horizontal turbulent diffusions of momentum, heat and moisture while Experiments 3 through 11 contain both horizontal and vertical turbulent diffusions of these quantities.

In Table I, $\overline{\theta}_I(p_o)$ is the reference potential temperature (K). The condensation interval is 5 time steps between successive applications of condensation and moist convective adjustment to the model in the moist experiments. Horizontal turbulent diffusion coefficients and initial boundary values of vertical turbulent diffusion coefficients (C_{mB}, $C_{\theta B}$, C_q) are relative humidity (percent) and initial static stability (K/cb).

Experiments were performed with a reference potential temperature ($\overline{\theta}_I(p_o)$), of 280K, 290K and 300K to simulate physically realistic situations. Changes to the dry atmosphere with different reference temperatures were almost negligible, but due to the exponential function in the Clausius-Clapeyron equation important differences were observed in the moist atmosphere.

Experiments were also conducted using different boundary values of vertical turbulent diffusion coefficients of momentum and heat.

The final experiment included a turbulent mixing coefficient which reduced the values of C_{mB} and $C_{\theta B}$ linearly to .1 of their original values between approximately the 93- and 84-cb levels in five equal steps.

The adjusted values of vertical turbulent diffusion coefficients of momentum C_m and heat C_θ were then varied as described by equations (5.1) and (5.2).

Primary emphasis on analyses of experimental results was on contour plots from the IBM 360/67 computer. These results obtained for all 11 experiments are analyses at t = 4 days of the fields of u, q, θ and w. The entire vertical plane is shown from 100 to 10 cb in these plots. However, the outer portion of the domain between $|y|$ = 1200 km and $|y|$ = 1800 km is not shown.

Figures 1-3 show the initial fields of u, θ and w at reference potential temperature of 290 K used in the following experiments. Contour plots for experiments 1 and 2 are shown as figures 4-10. Figures 4 and 5 show distributions of the rotational wind, u for corresponding dry and moist experiments, respectively. Features of u at all levels differ quite significantly from dry to moist experiments. There is a marked increase in horizontal and vertical shear in the easterly flow in the moist experiment in the vicinity of the front near the surface. Horizontal and vertical wind shear is also more intense at low middle to middle levels in the

moist experiment. It is noteworthy that this property is dominant throughout the moist solutions. In the moist experiment the jet core increases in magnitude while shear decreases to zero at a lower level in the northern region near the tropopause. Figures 6 and 7 contrast values of θ throughout the domain. Noted is the warmer air in middle levels in the frontal zone. A slightly more intense gradient is seen near the surface with little change in tilt of the front. All this is attributed to the latent heat release in the moist experiment 2.

Vertical motions for the experiments are investigated in Figures 8 and 9. Upward vertical motions occupy a much larger zone, extend much higher and occur closer to the frontal zone in the warm air mass of the moist experiment. Significant downward motion occurs between $|Y| = 1200$ and $|Y| = 1800$ km (not shown in the figures).

Figure 10 shows the field of specific humidity for experiment number 2. Maximum precipitation is .37 inches. Figures 11 through 17 compare the dry and moist fields of u, θ and w and show the q fields of experiments 3 and 4. Figures 11 and 12 show a small increase in the zone of easterly component in the lower levels of the moist experiment. Vertical and horizontal shear are also seen to increase as in experiments 1 and 2. Also noted is a much larger jet core in the moist experiment, with a slight northward shift. Noteworthy is a significant decrease in magnitude of the easterly component of u near the surface from that of experiments 1 and 2. Figures 13 and 14 exhibit

the same contrast in potential temperature as that of experiments 1 and 2. It is noted that the air at low levels and near the tropopause is colder in the moist experiment with vertical turbulent diffusion added (exp. 4). This is also true in the dry experiments. This is attributed to the increased amount of heat loss due to the vertical turbulent diffusion of momentum and heat offsetting the release of latent heat in the moist experiments. The air at mid levels in the frontal zone is warmer in the moist experiment as seen before. Figures 15 and 16 show a marked change in vertical motion between dry and moist experiments. A large zone of upward motion is seen near the frontal zone with maximum values exceeding 3×10^{-3} mb/sec near the 85-cb level. Figure 17 shows the specific humidity of experiment 4. Noteworthy is the dramatic shift to the south in specific humidity following the frontal position.

Figures 19 through 38 compare the moist and dry fields of u, θ and w and show the specific humidity of the moist experiments using boundary values of vertical turbulent diffusion of heat and momentum of .0007 cb^2sec^{-1} (5 m^2sec^{-1} in height coordinates) at reference potential temperatures of 290, 280 and 300 K.

Figures 18 and 19 contrast the u field of experiments 5 and 6 at $\overline{\theta}_I(p_o)$ = 290 K. Noteworthy is the increase in zone of maximum easterly component of the wind at low levels and the more intense horizontal and vertical shear in low levels over experiments 3 and 4. A slight northward shift and increase in size of the jet core is noted in the moist experiment.

Figures 20 and 21 show little difference in potential temperature fields, although the air in the frontal zone in middle levels is warmer in the moist experiment due latent heat release. There is a marked increase in tilt of the front over previous experiments, due to more normal northward position of the front at the surface. Figures 22 and 23 contrast the vertical motion of experiments 5 and 6 showing a maximum in upward motion near the 850-mb level consistent with previous experiments. Figure 24 shows the specific humidity field which differs slightly more in the same manner as experiment 4 differed from 2. Maximum precipitation is .4 in.

Figures 25 and 26 show more intense horizontal and vertical shear apparent in the easterly component of the moist experiment at $\overline{\theta}_I(p_o)$ = 280 K. The jet core is reduced in size and magnitude from experiments 5 and 6 and the horizontal shear decreases significantly near the tropopause. It should be noted here that the tropopause in experiments 7 and 8 is lower than the tropopause in previous and subsequent experiments due to the lower reference potential temperature used. Figures 27 and 28 show little difference between moist and dry fields of potential temperature except for the warmer air in mid levels in the frontal zone of the moist experiment due latent heat release. Noteworthy in these experiments 7 and 8 is the zone of low stability and apparent break in the tropopause in the northern part of the region. Figures 29 and 30 show a similar contrast between

moist and dry fields of vertical motion as seen in previous experiments except that the contrast is not as dramatic as seen before. Figure 31 shows the q field is reduced considerably over previous experiments due to the lower reference potential temperature used (280 K). Maximum precipitation reduced to .15 inches.

Figures 32 through 40 show a much higher tropopause due to the larger reference potential temperature (300 K). A dramatic change in the u field is seen in Figures 32 and 33 between dry and moist fields. Especially noteworthy is the very strong jet core and much more intense horizontal and vertical wind shear. Also note a large shift in the jet to the north which was not quite so obvious in previous experiments. Figures 34 and 35 also show a marked contrast between dry and moist potential temperature fields. The air is much warmer in the upper levels near the tropopause due to the latent heat release. Thermal gradients along the frontal zone are also stronger in the mid and upper levels. Strong heating in upper levels is apparent. Vertical motions (Figures 36 and 37) exceed 3×10^{-3} mb/sec in the warm moist air. The contrast is similar to that seen in previous experiments. The moisture field (Figure 38) is greatly intensified over previous experiments and specific humidities are in excess of 19 g/kg at low levels to the south. This is no doubt due to the larger quantities of latent heat release observed in this experiment, and the larger initial reference potential temperature. Maximum precipitation increased to .71 inches.

Figures 39 and 42 show experiment 11 which included the turbulent mixing coefficient into experiment 4. The only differences noted were a small pocket of lower specific humidity (Figure 42) at the top of the mixing level and a decreased zone of maximum upward motion in the warm moist air of the mixed experiment (Figure 41). From the above we conclude that vertical turbulent mixing has no effect on mid and upper level deformation fields.

Comparison of the results of the previous experiments with similar experiments of Cornelius [1974] revealed the following:

1. The westerly wind field extended much lower while the easterly wind field was compressed below the 85 cb level. The zero wind level was also observed to be lower in the expanded atmosphere with tropopause included. This is true in both moist and dry experiments. The jet was also lower and more apparent.

2. The pockets of warm air were apparent in the frontal zone as in Cornelius [1974], but frontal tilt was somewhat less after 4 days in the experiments conducted in this study.

3. Significant downward vertical motion occurred outside the zone observed in both studies although larger values are evident in the studies of Cornelius [1974].

4. Specific humidity fields were similar in both studies.

VI. CONCLUSIONS AND RECOMMENDATIONS

The numerical model of Williams [1974] is modified in this study to include moisture, a tropopause and lower stratosphere and variable vertical turbulent diffusion of heat and momentum. This leads to a more realistic situation and consequently more realistic solutions. Intensification of the baroclinic zone is seen to occur in upper levels, although no effect is apparent on the surface due to the inclusion of moisture. The effects of vertical turbulent diffusion is apparent throughout the frontal zone through increased tilt, reduced heating and reduced values of windspeed. The expanded boundary and inclusion of the tropopause along with a conversion to $\ell n\ p$ vertical spacing tended to shift all features to a lower level in the domain. Jet cores were generally larger and vertical motions increased in the warm moist air near the frontal zone due to the heating. The moist models illustrate an exponential thermal dependence in the various experiments at the reference potential temperatures of 280, 290 and 300 K.

In future studies using this model, attention should be directed toward the use of still more realistic boundaries, such as a higher upper boundary. A translational motion should be added to the system so that warm and cold frontal effects could be investigated. Finally, an improved convective scheme such as that of Arakawa and Schubert [1973] could be applied to the model.

Table I.

EXP NO.	$\bar{\theta}_I(p_o)$ °K	MOIST OR DRY	A_M m^2/sec	A_θ m^2/sec	A_q m^2/sec	C_{mB} cb^2/sec	$C_{\theta B}$ cb^2/sec	C_q cb^2/sec	RH %	$\partial\bar{\theta}_I/\partial p$ °K/cb
1	290	D	30,000	30,000	100,000	0	0	0	0	-.53
2	290	M	30,000	30,000	100,000	0	0	0	70	-.53
3	290	D	30,000	30,000	100,000	.0014	.000176	0	0	-.53
4	290	M	30,000	30,000	100,000	.0014	.000176	0	70	-.53
5	290	D	30,000	30,000	100,000	.0007	.0007	0	0	-.53
6	290	M	30,000	30,000	100,000	.0007	.0007	0	70	-.53
7	280	D	30,000	30,000	100,000	.0007	.0007	0	0	-.53
8	280	M	30,000	30,000	100,000	.0007	.0007	0	70	-.53
9	300	D	30,000	30,000	100,000	.0007	.0007	0	0	-.53
10	300	M	30,000	30,000	100,000	.0007	.0007	0	70	-.53
11	290	M	30,000	30,000	100,000	.0014	.000176	0	70	-.53
	290	D	Initial							

Table II. Forecast Levels (cb)

LEVEL	p(cb)		p(cb)		p(cb)
1	95.86	19	44.81	37	20.95
2	91.9	20	42.96	38	20.08
3	88.1	21	41.18	39	19.25
4	84.45	22	39.48	40	18.25
5	80.96	23	37.85	41	17.69
6	77.61	24	36.28	42	16.96
7	74.4	25	34.78	43	16.26
8	71.32	26	33.34	44	15.59
9	68.37	27	31.96	45	14.94
10	65.54	28	30.64	46	14.32
11	62.83	29	29.37	47	13.73
12	60.23	30	28.16	48	13.16
13	57.54	31	26.99	49	12.62
14	55.35	32	25.88	50	12.10
15	53.06	33	24.81	51	11.60
16	50.87	34	23.78	52	11.12
17	48.76	35	22.80	53	10.66
18	46.75	36	21.85	54	10.22

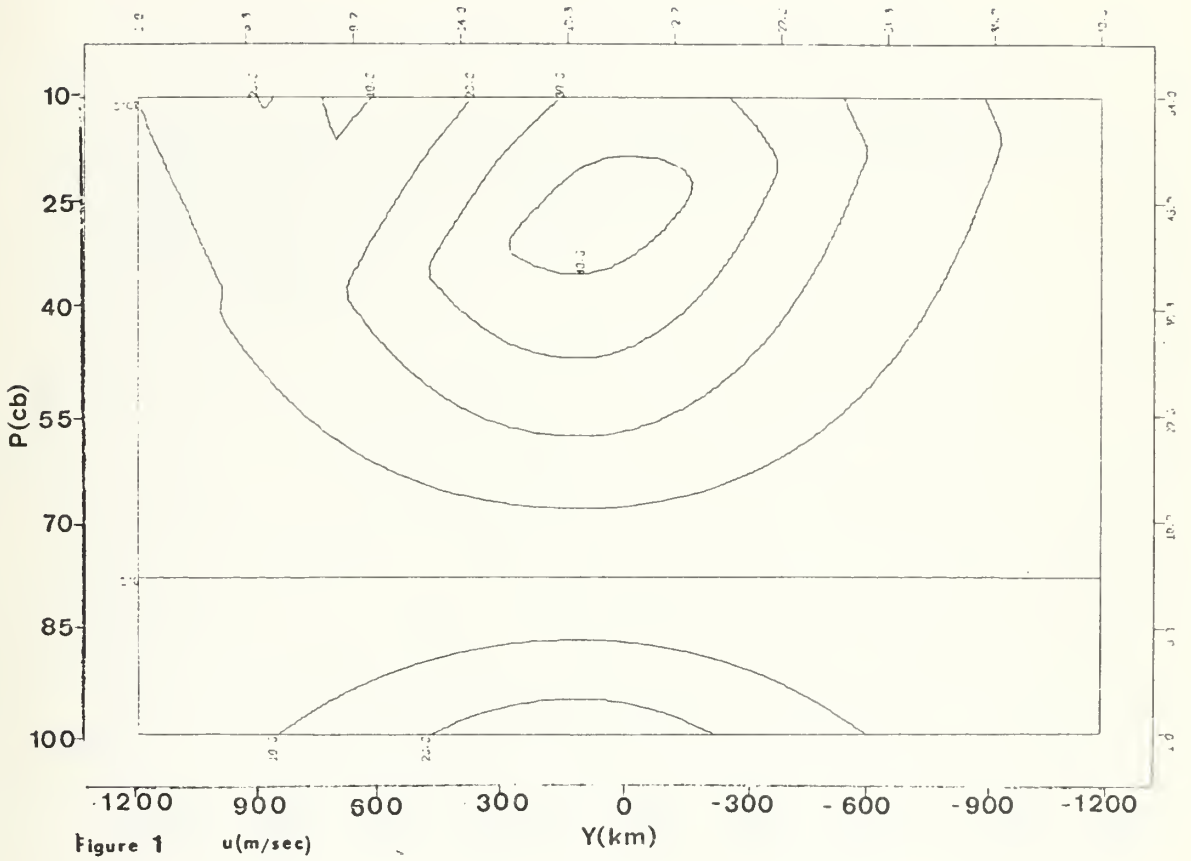

Figure 1 u(m/sec)

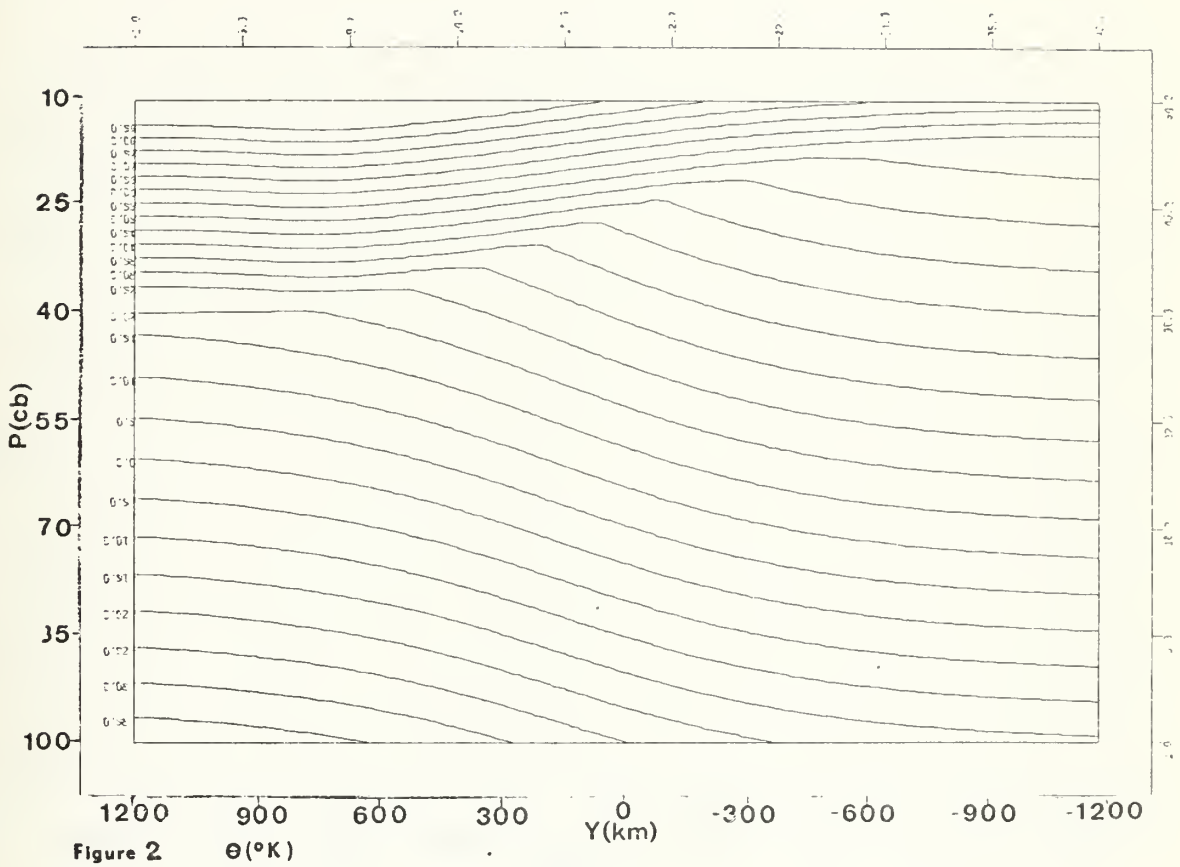

Figure 2 θ(°K)

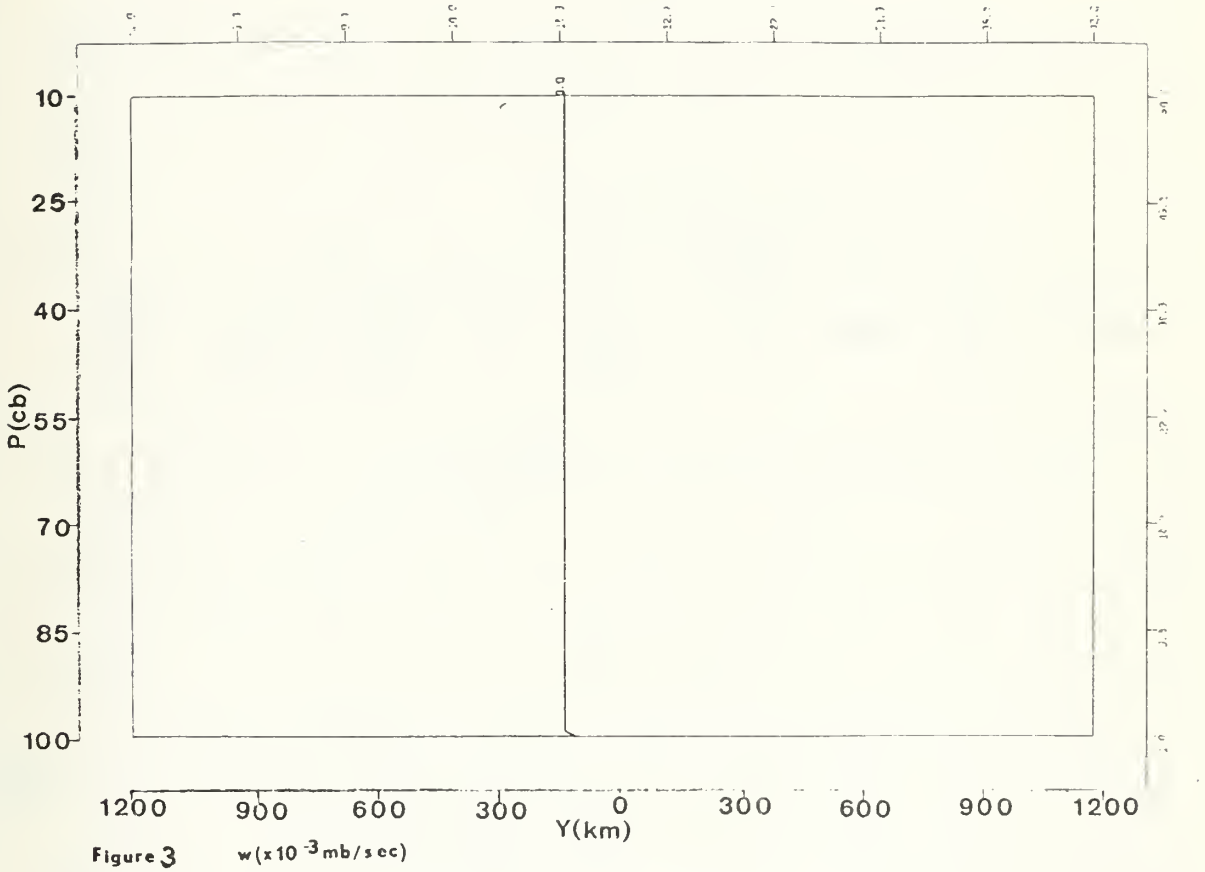

Figure 3 w(x10 $^{-3}$mb/sec)

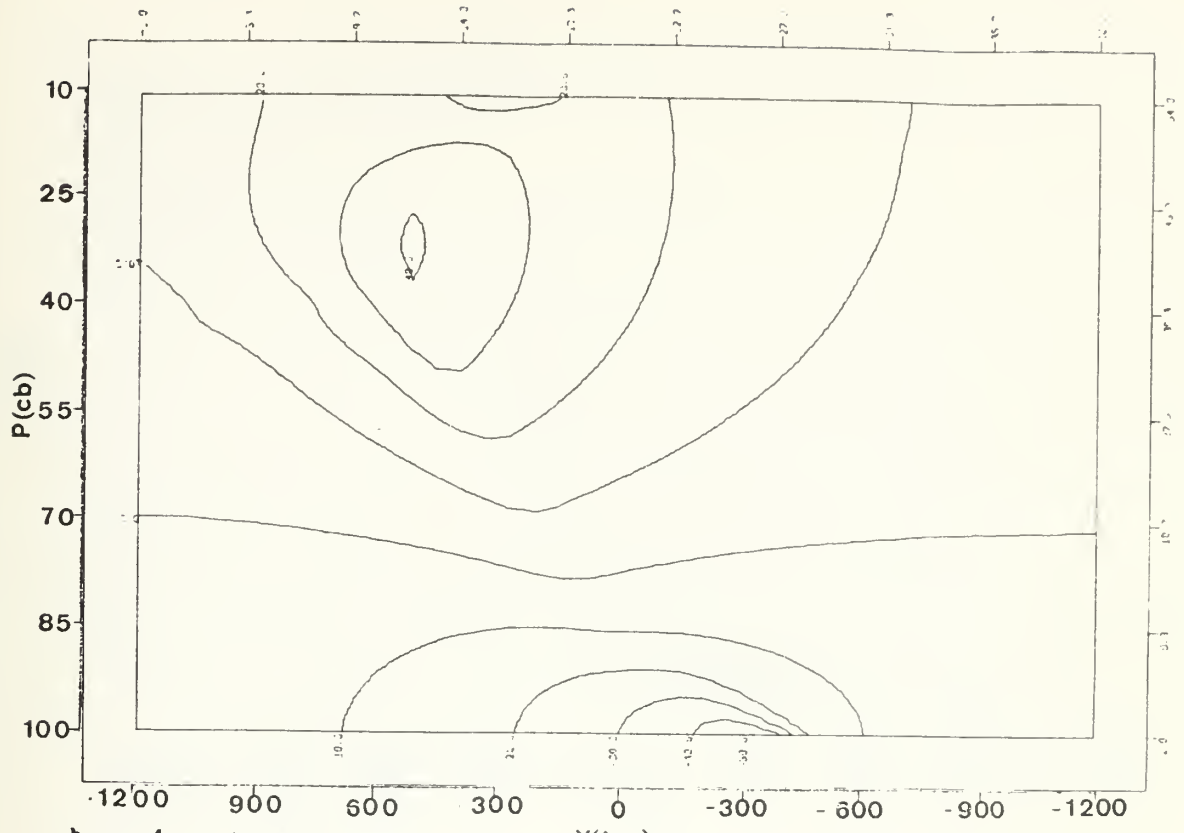

Figure 4 u(m/sec) Exp.1

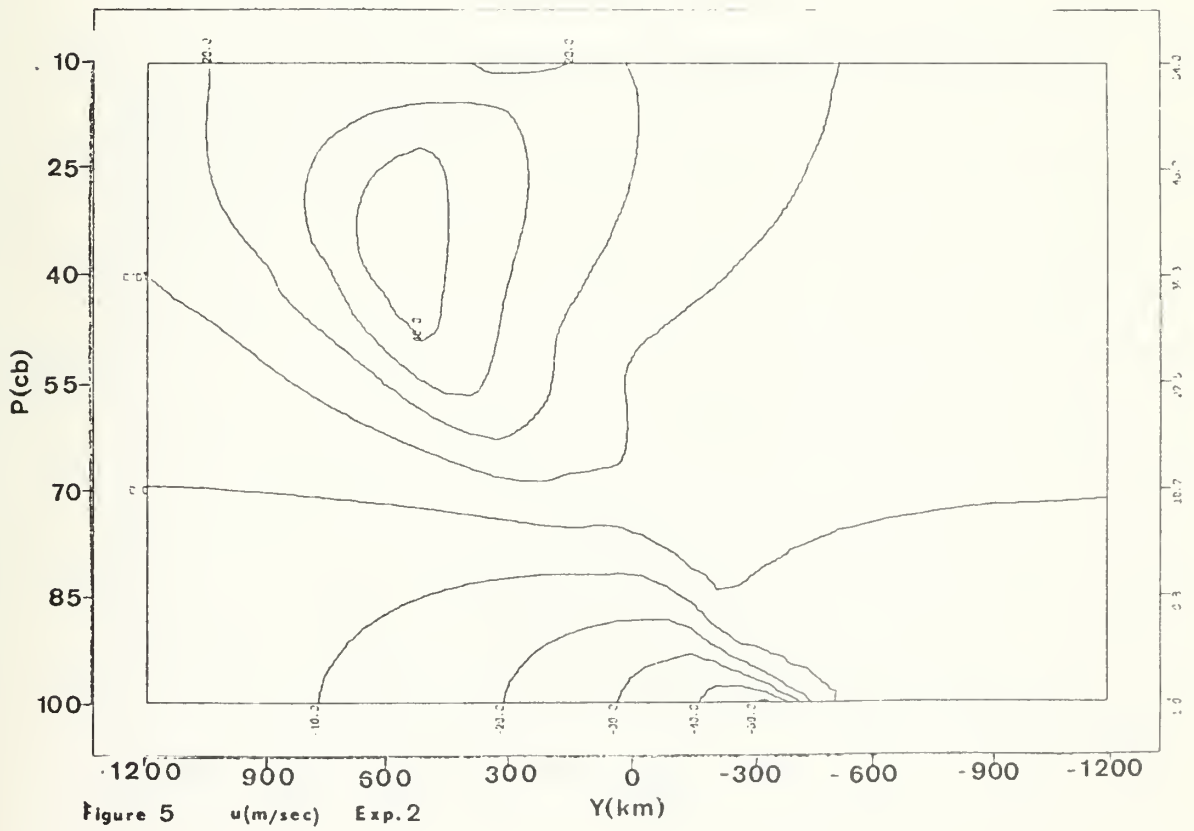

Figure 5 u(m/sec) Exp.2

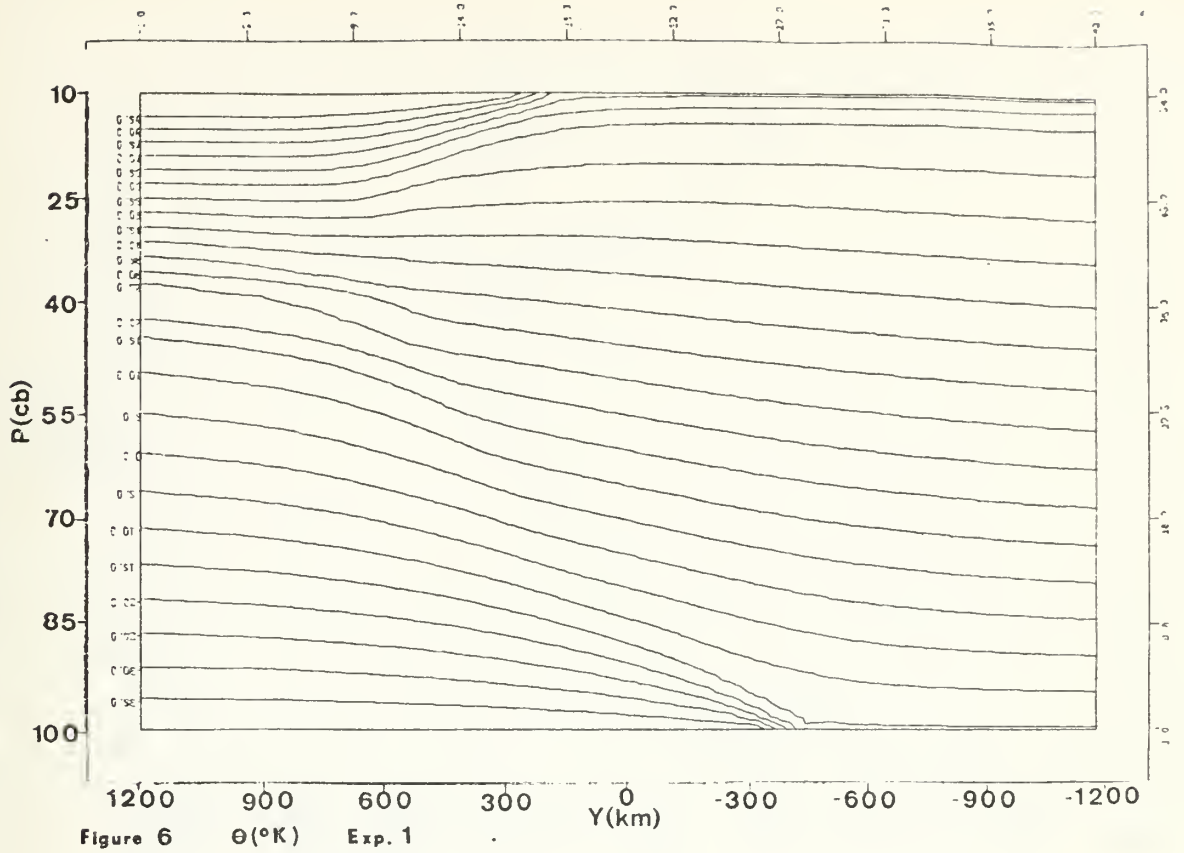

Figure 6 Θ(°K) Exp. 1

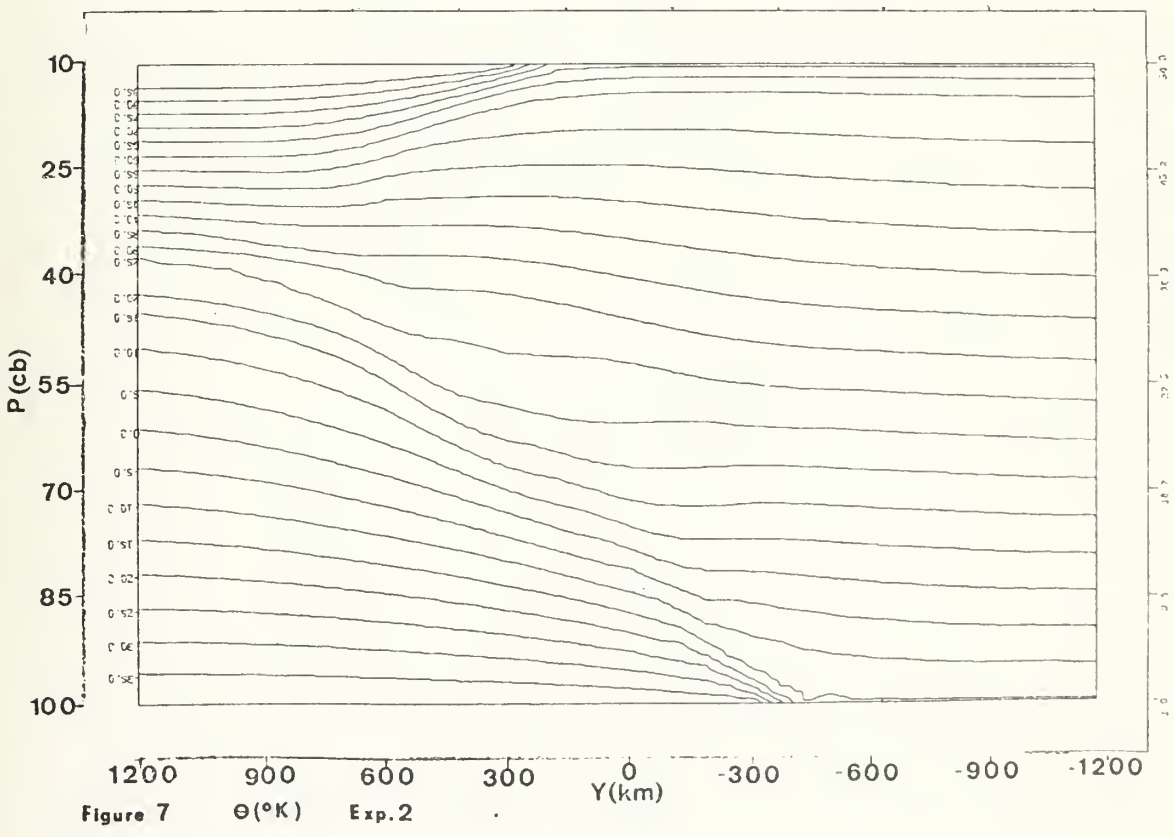

Figure 7 Θ(°K) Exp.2

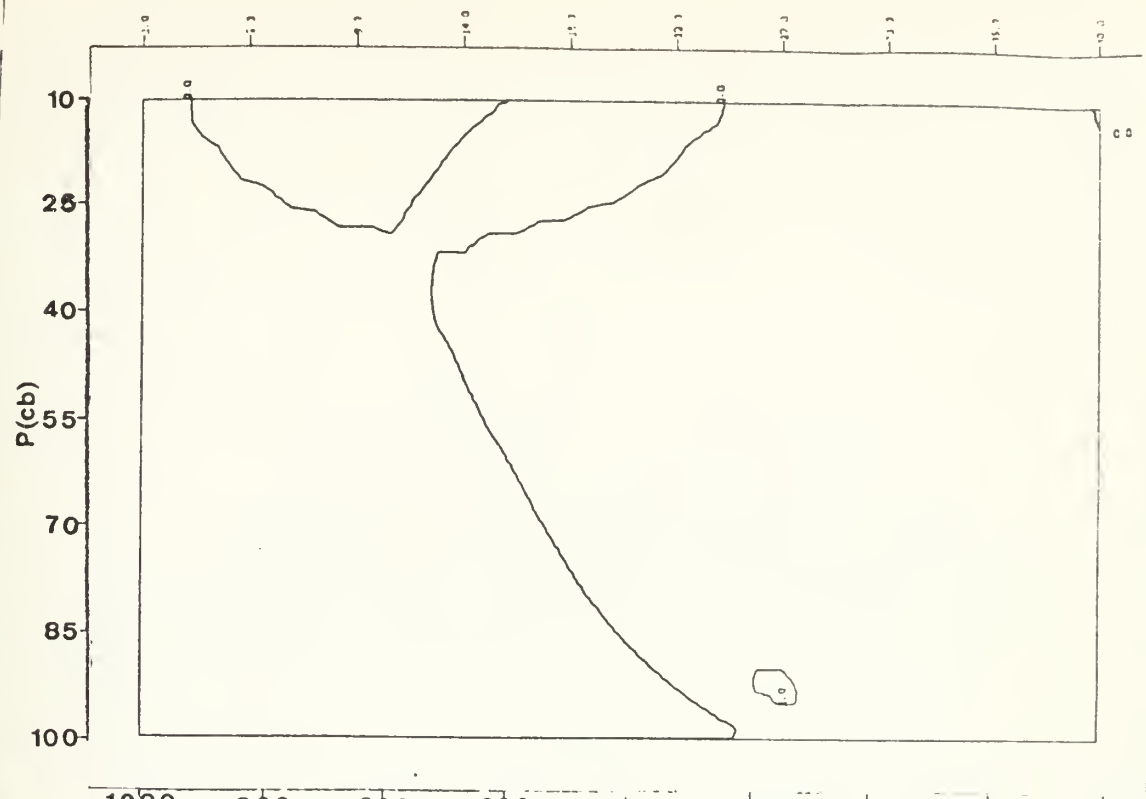

Figure 8 w(x10 $^{-3}$mb/sec) Exp.1

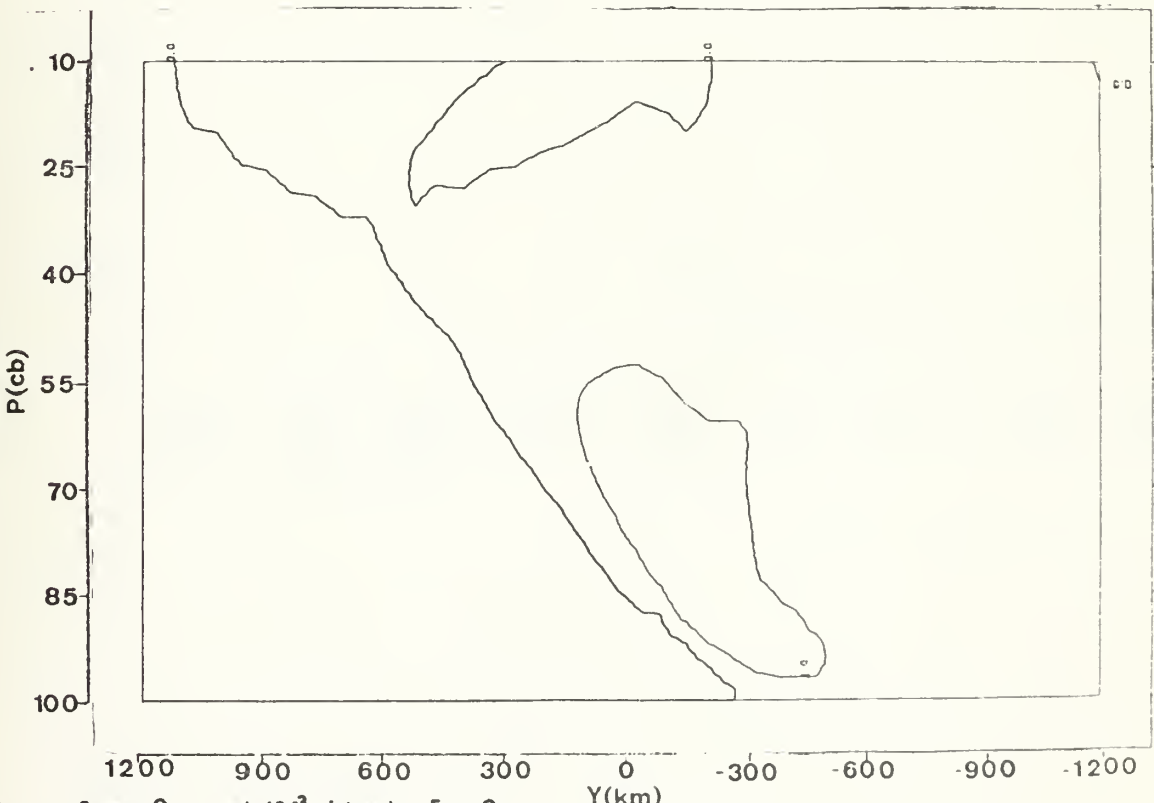

Figure 9 w(x10 $^{-3}$mb/sec) Exp.2

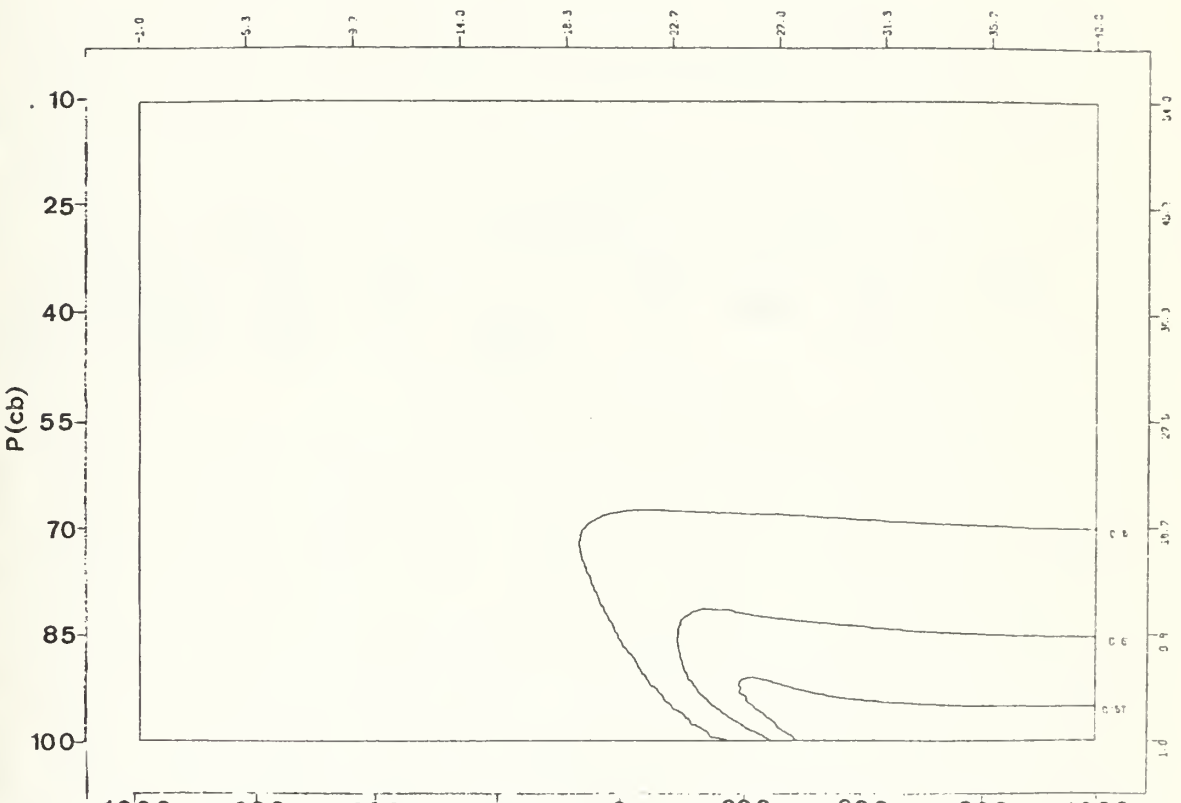

Figure 10 q(g/kg) Exp. 2

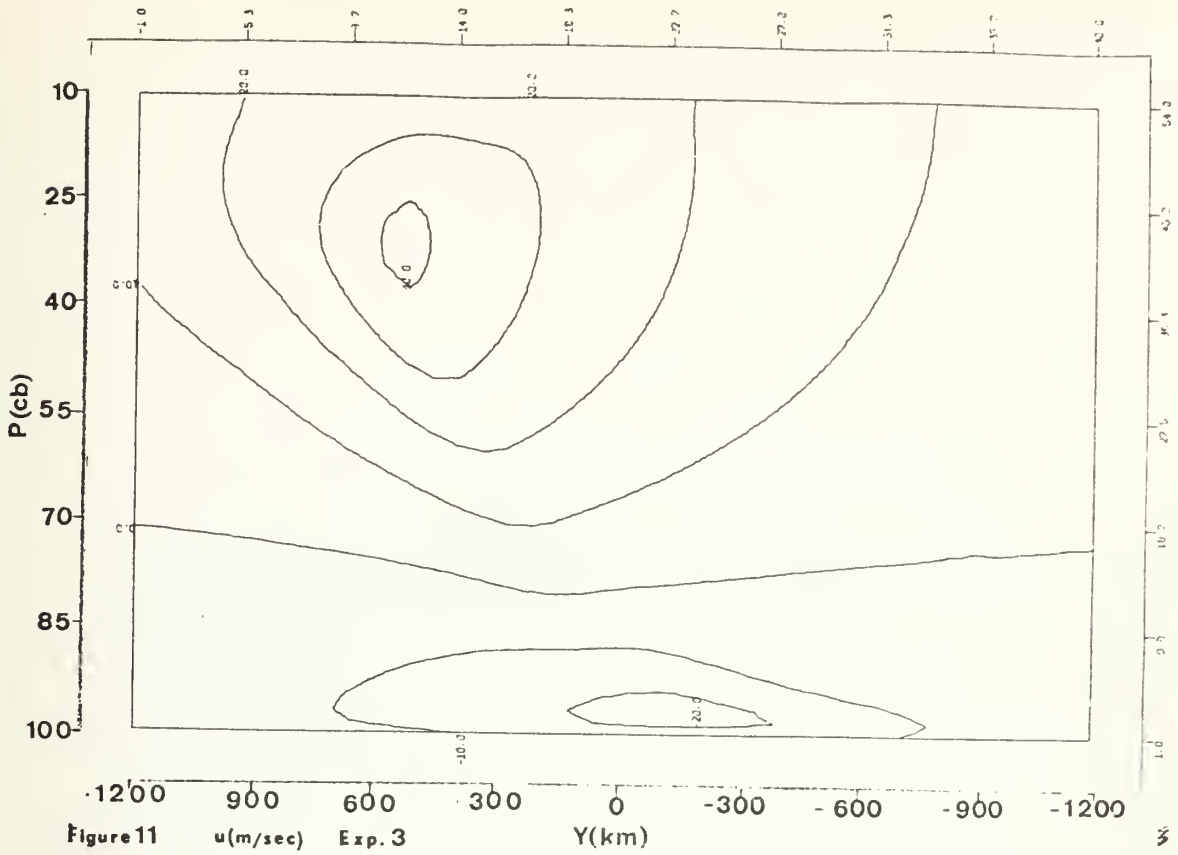

Figure 11 u(m/sec) Exp. 3

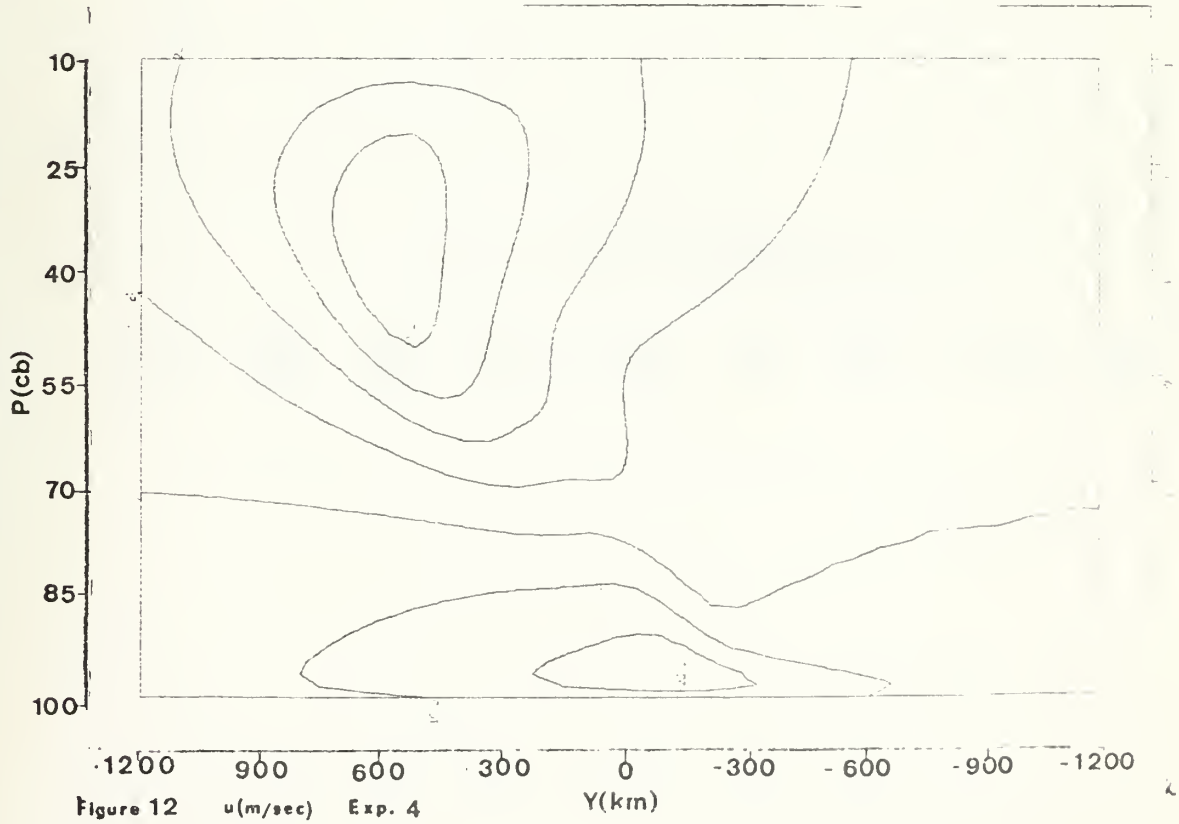

Figure 12 u(m/sec) Exp. 4

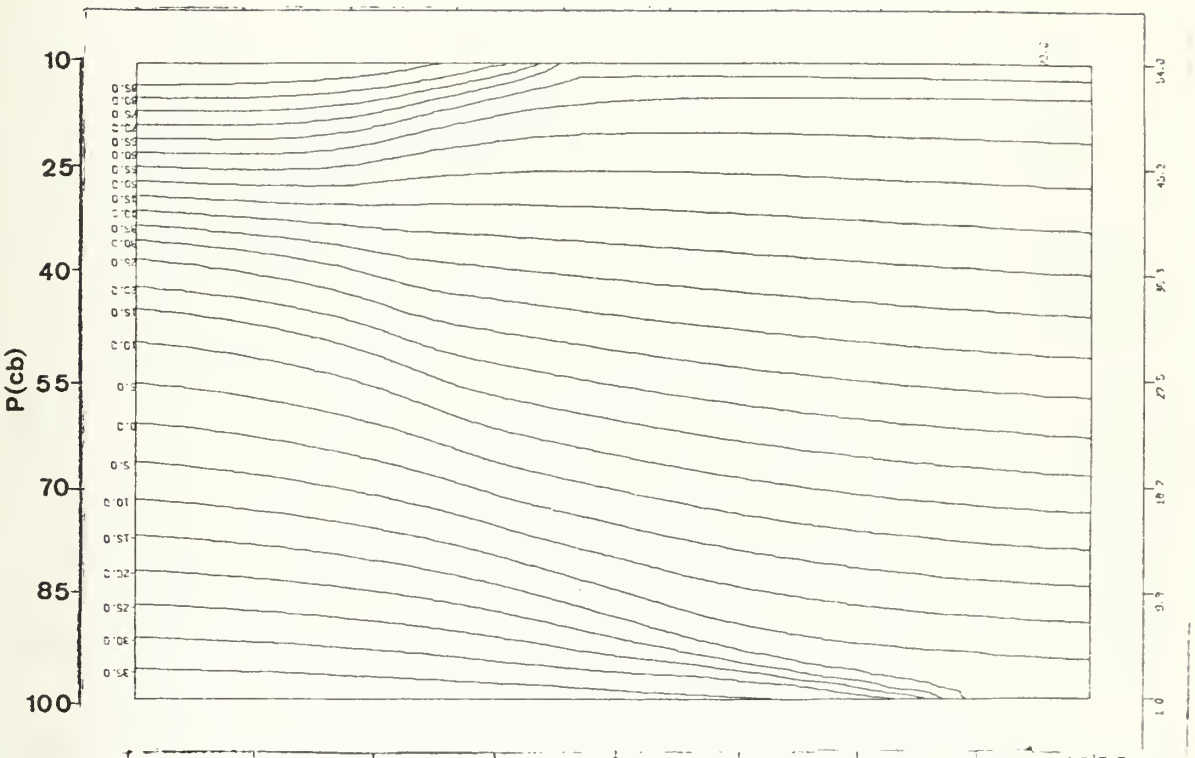

Figure 13 Θ(°K) Exp. 3

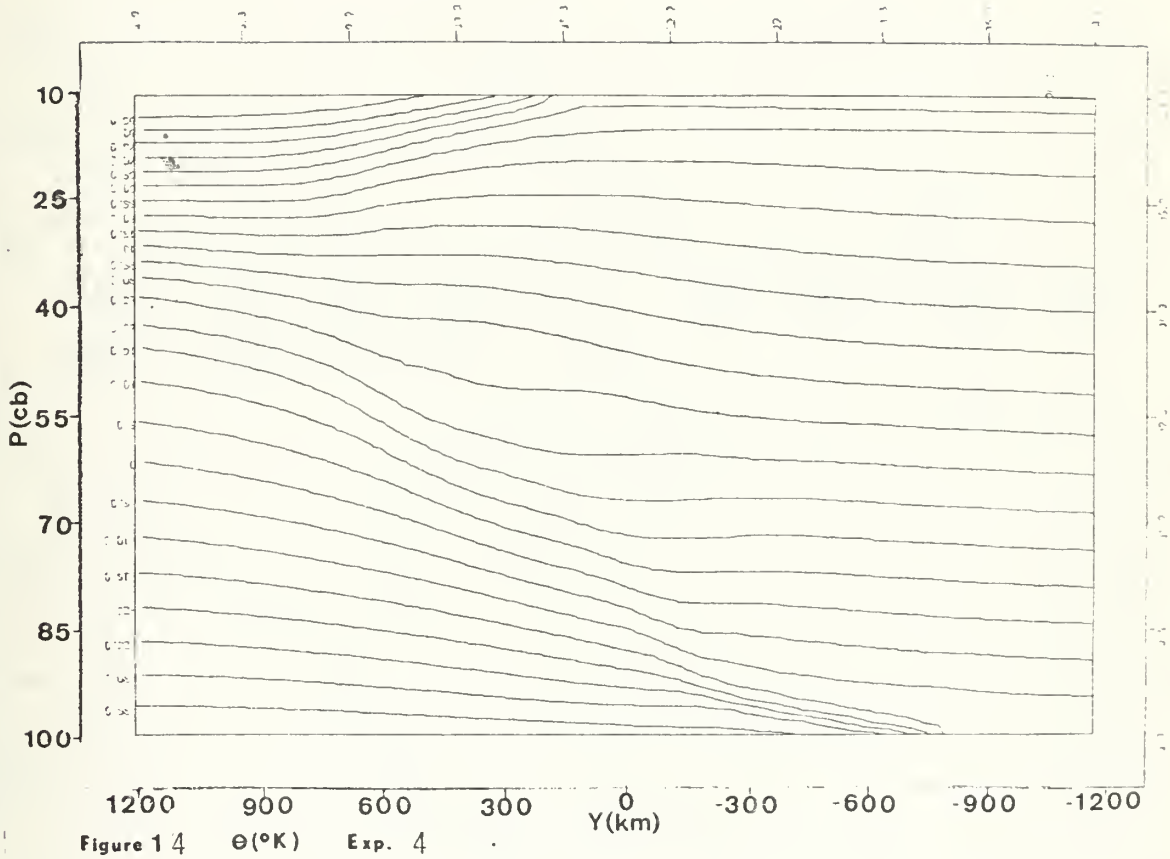

Figure 14 Θ(°K) Exp. 4

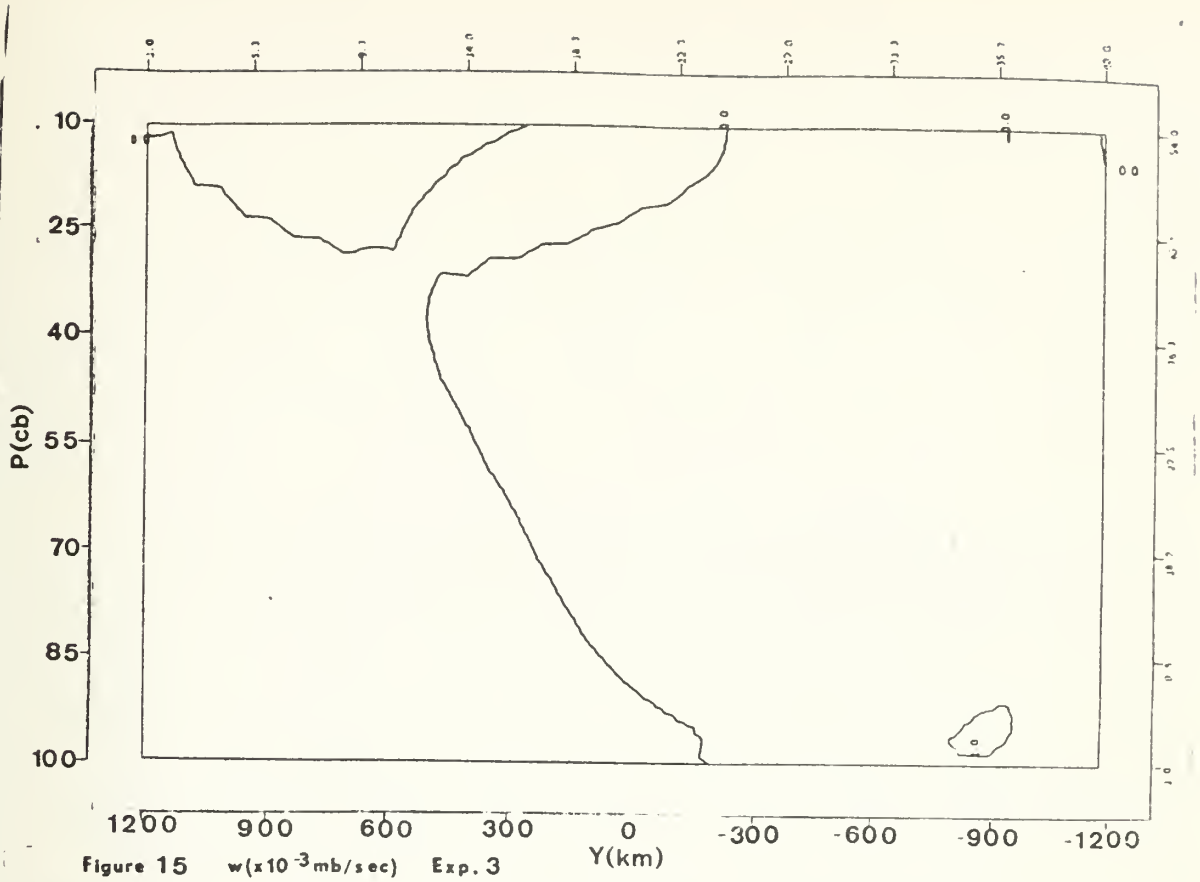

Figure 15 w(x10 $^{-3}$mb/sec) Exp. 3

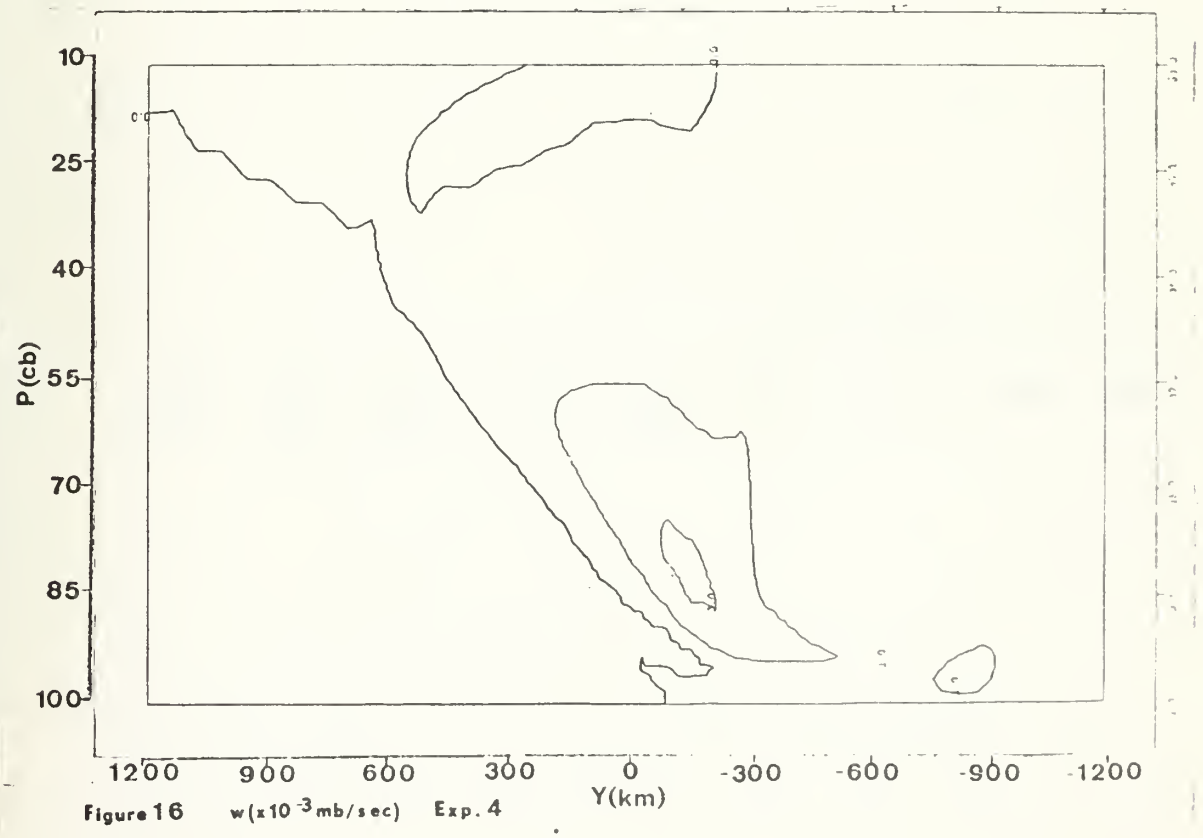

Figure 16 w(x10 $^{-3}$mb/sec) Exp. 4

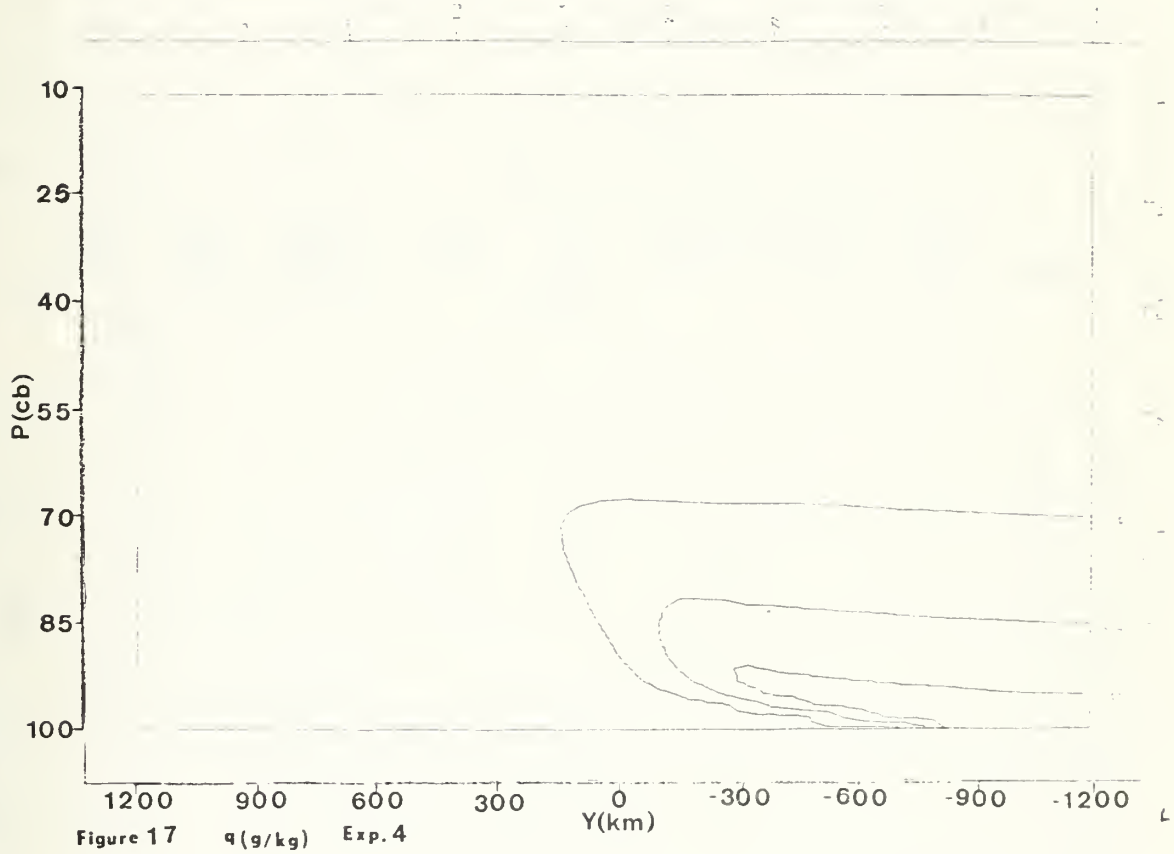

Figure 17 q(g/kg) Exp. 4

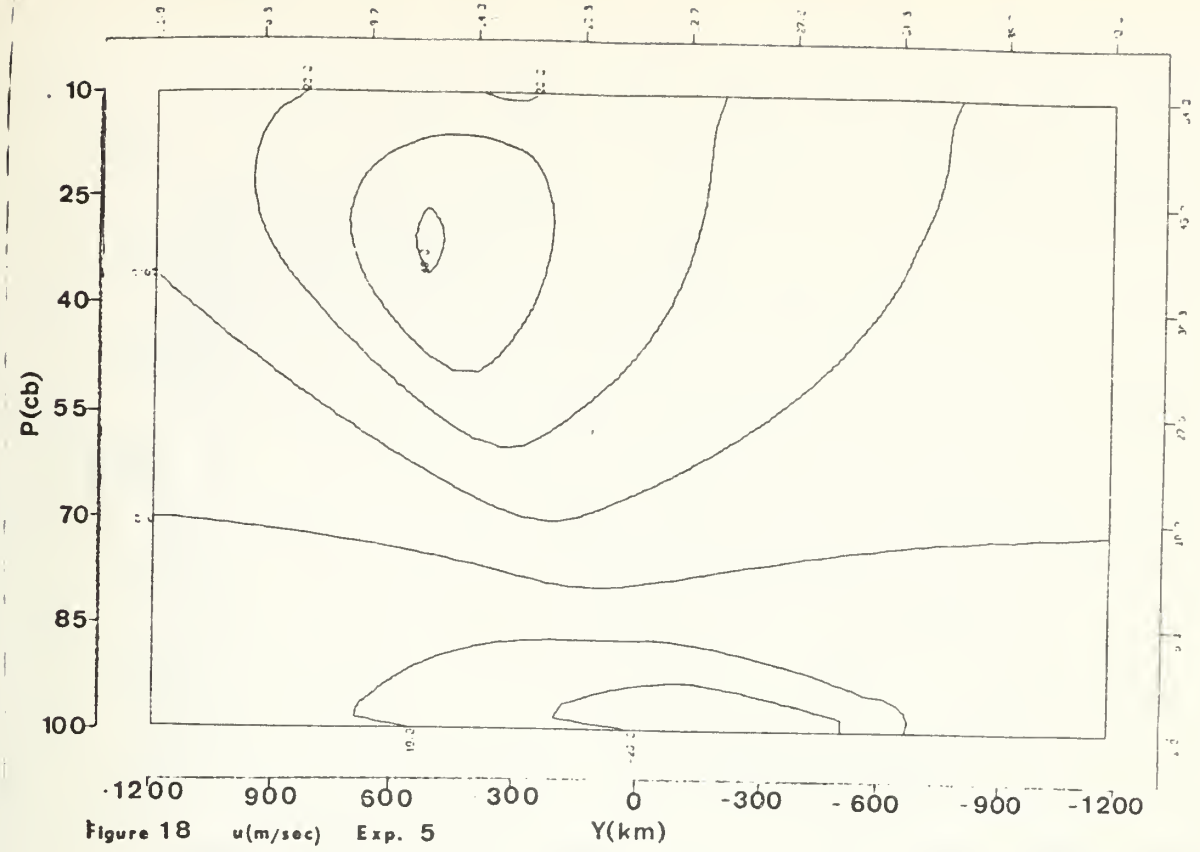

Figure 18 u(m/sec) Exp. 5

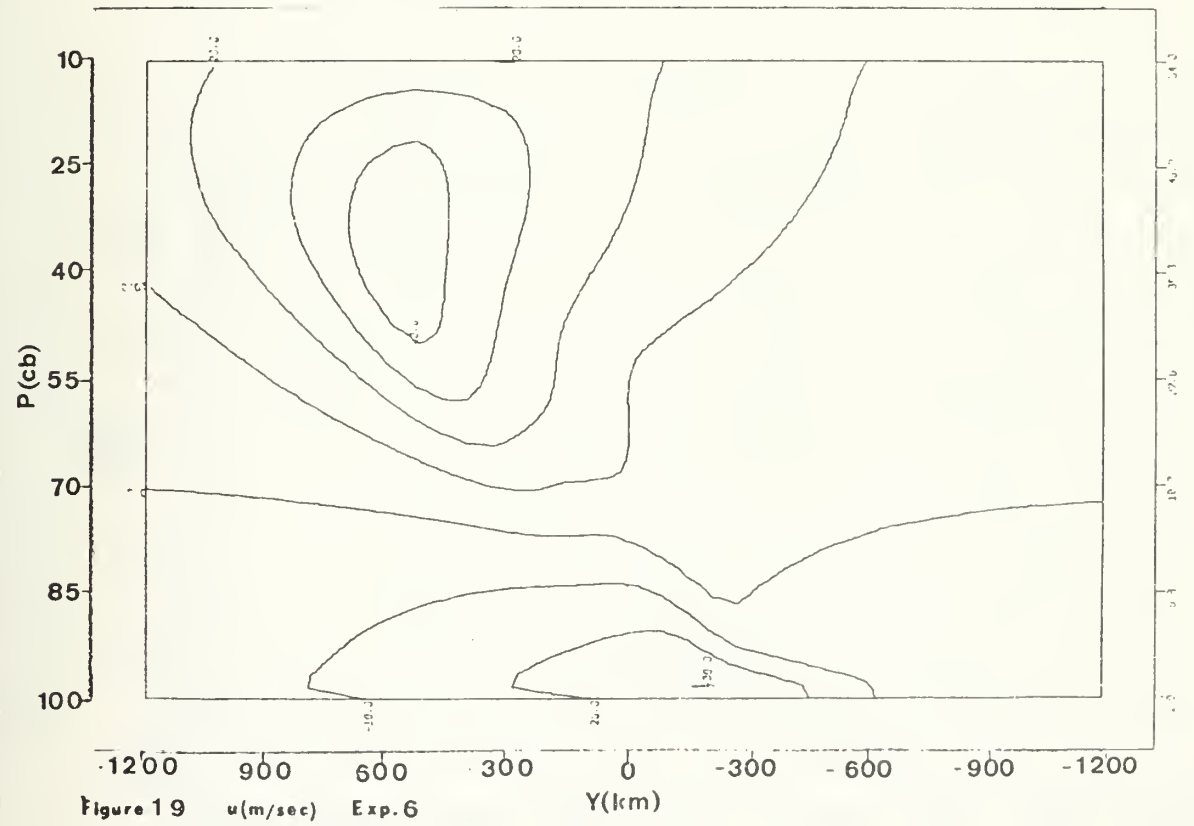

Figure 19 u(m/sec) Exp. 6

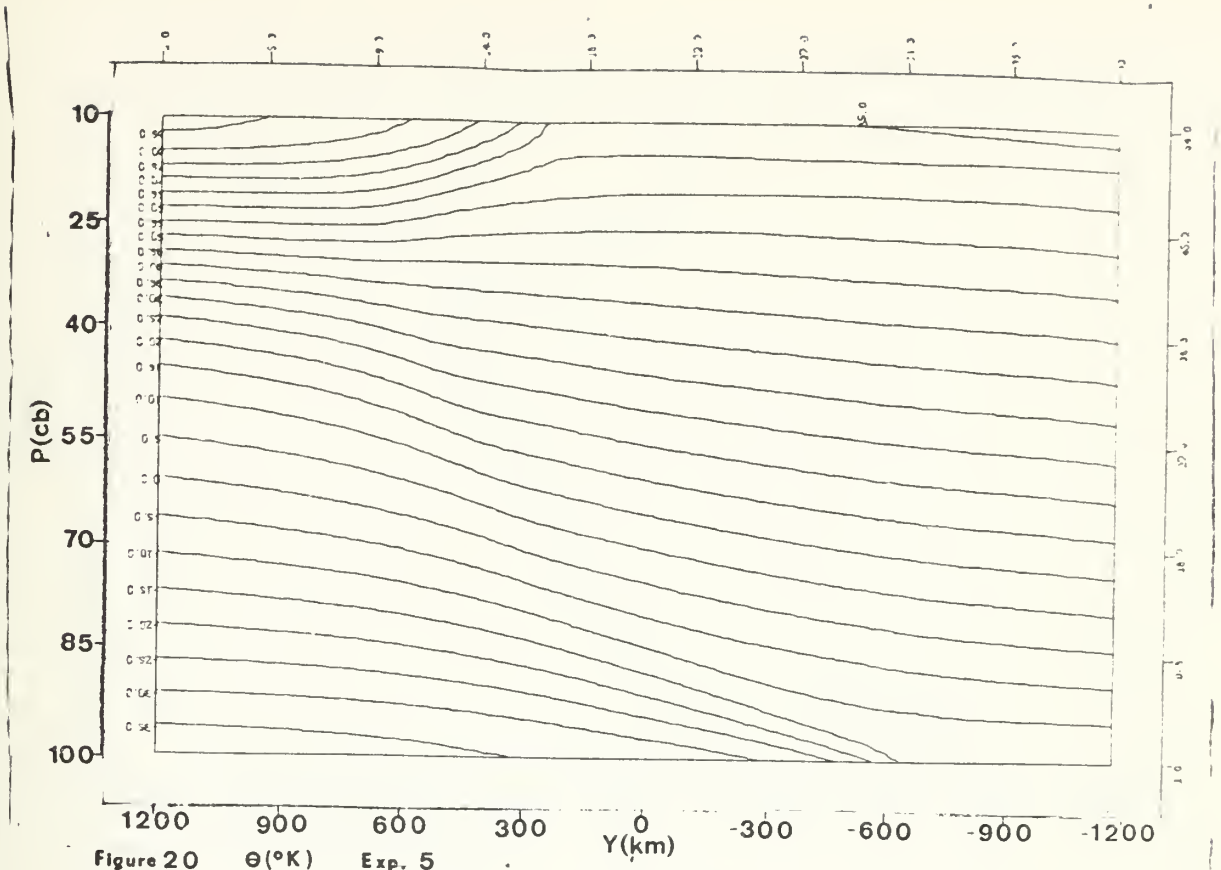

Figure 20 Θ(°K) Exp. 5

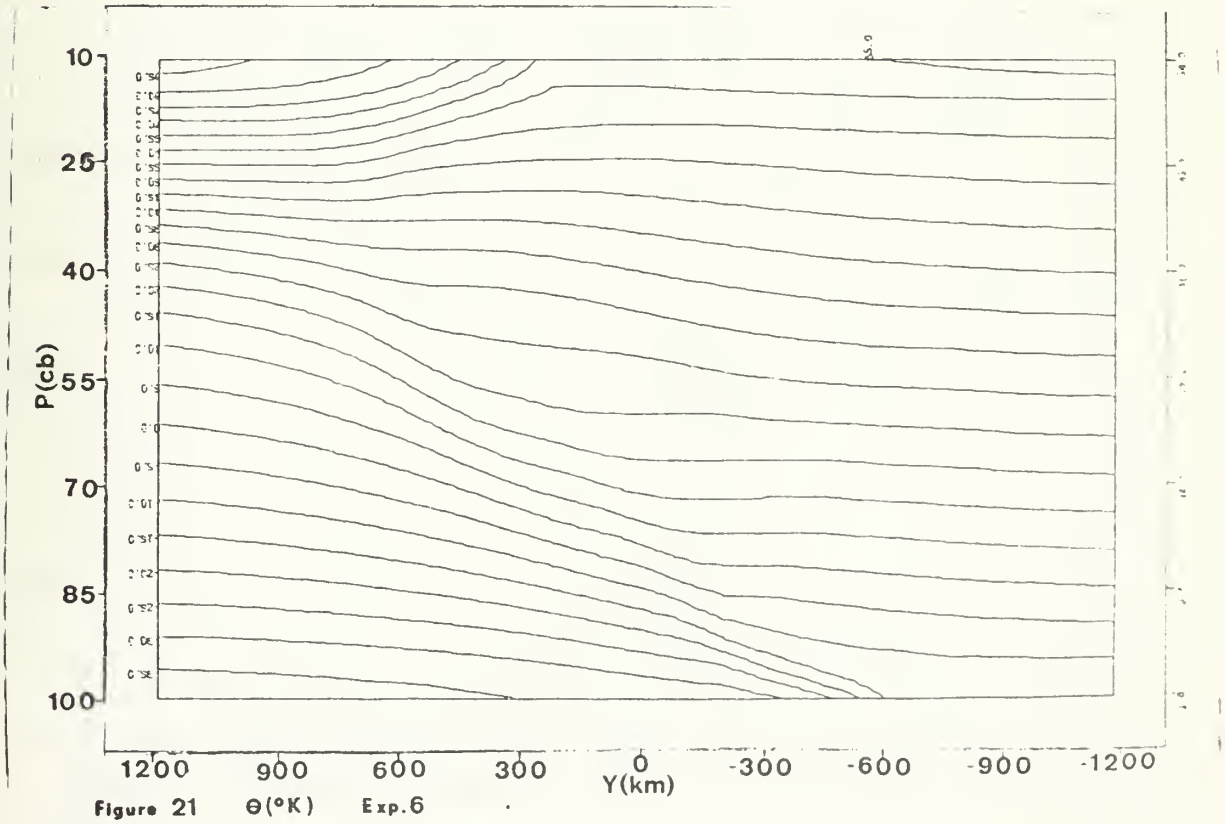

Figure 21 Θ(°K) Exp.6

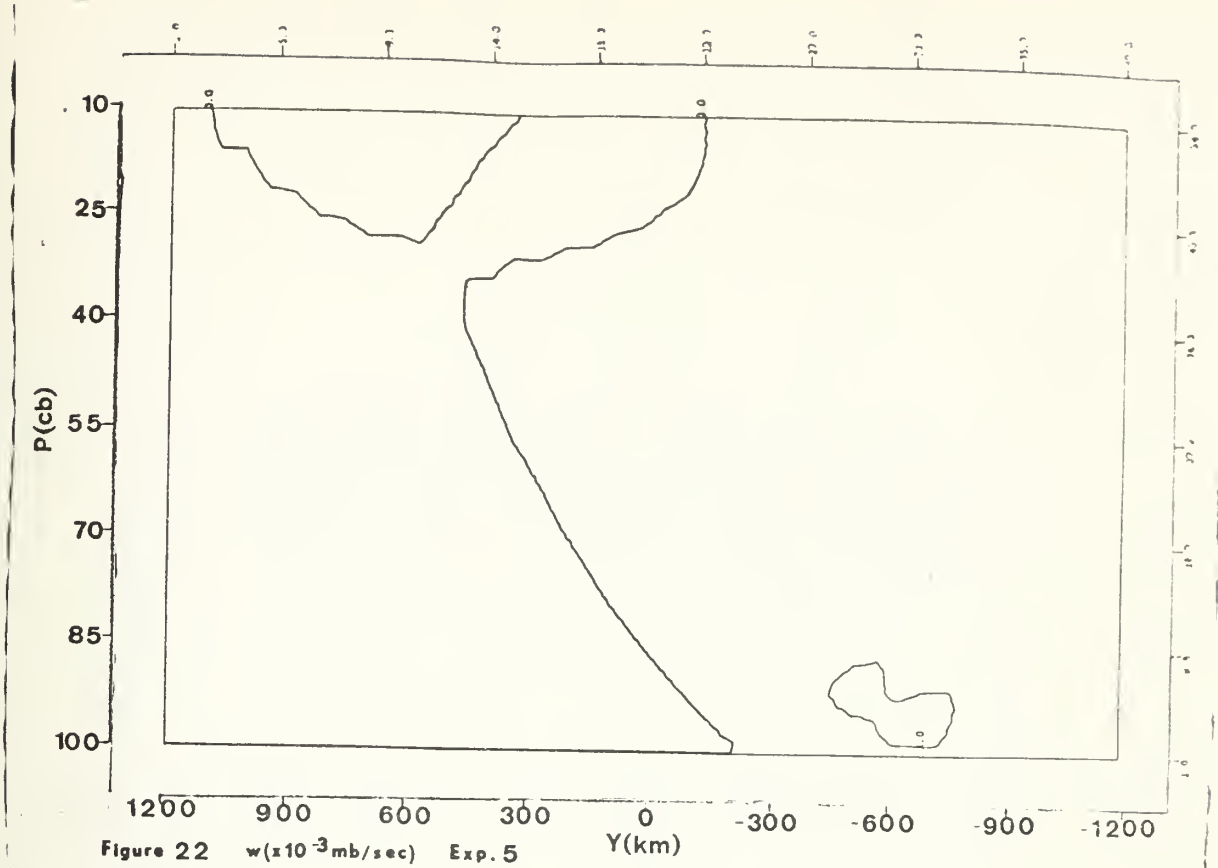

Figure 22 w(x10 $^{-3}$mb/sec) Exp. 5

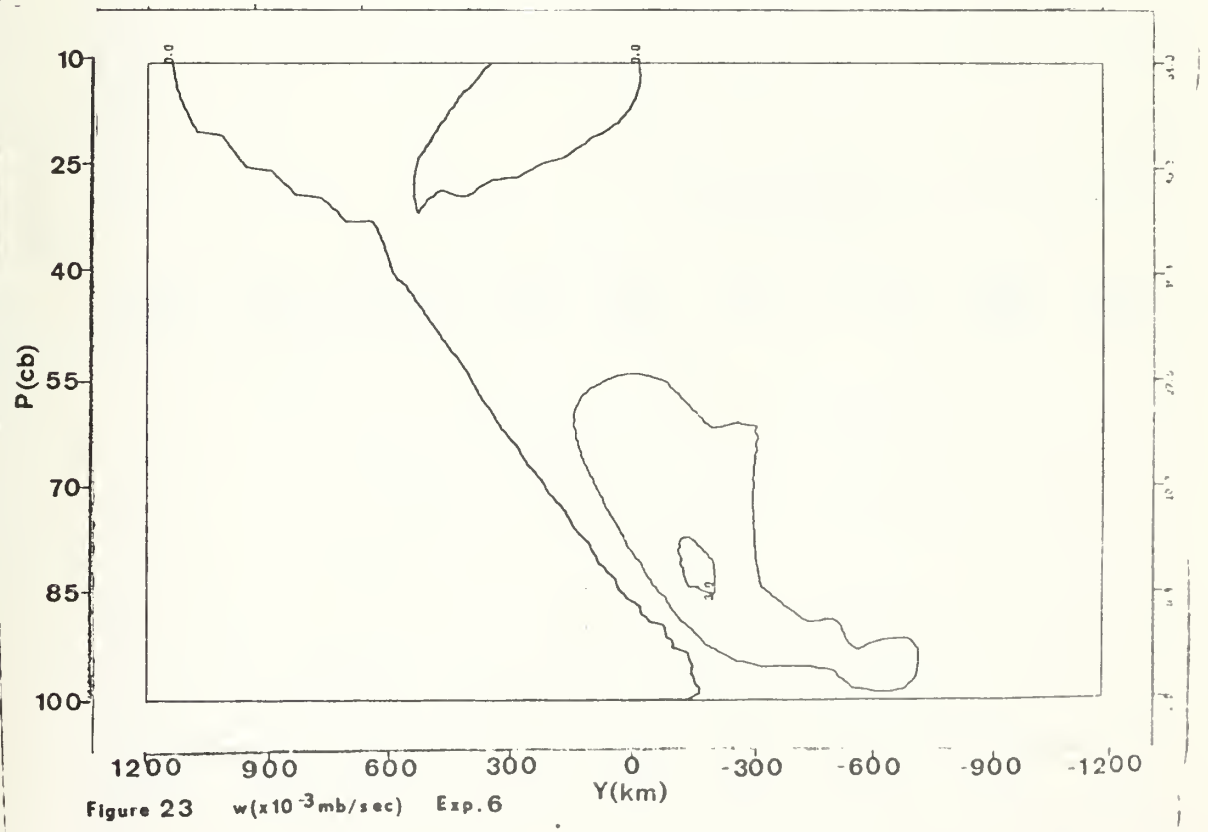

Figure 23 w(x10 $^{-3}$mb/sec) Exp. 6

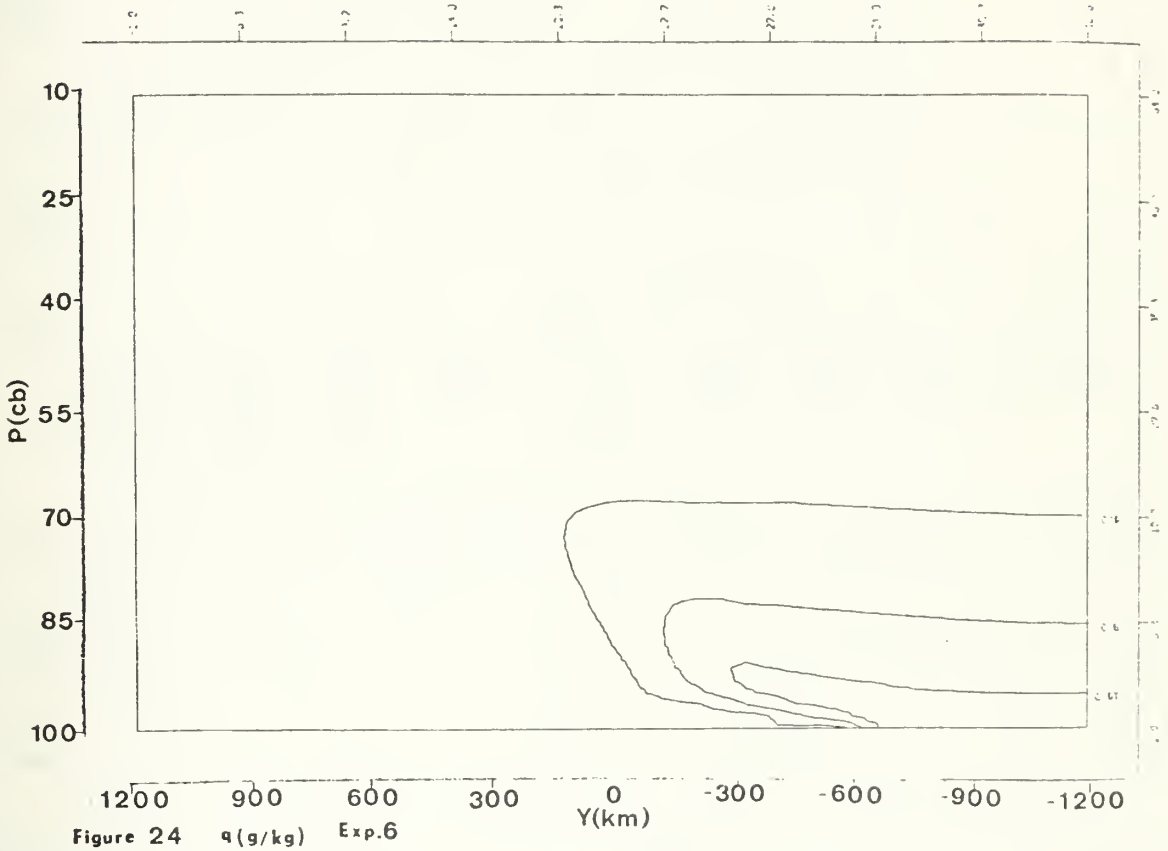

Figure 24 q(g/kg) Exp.6

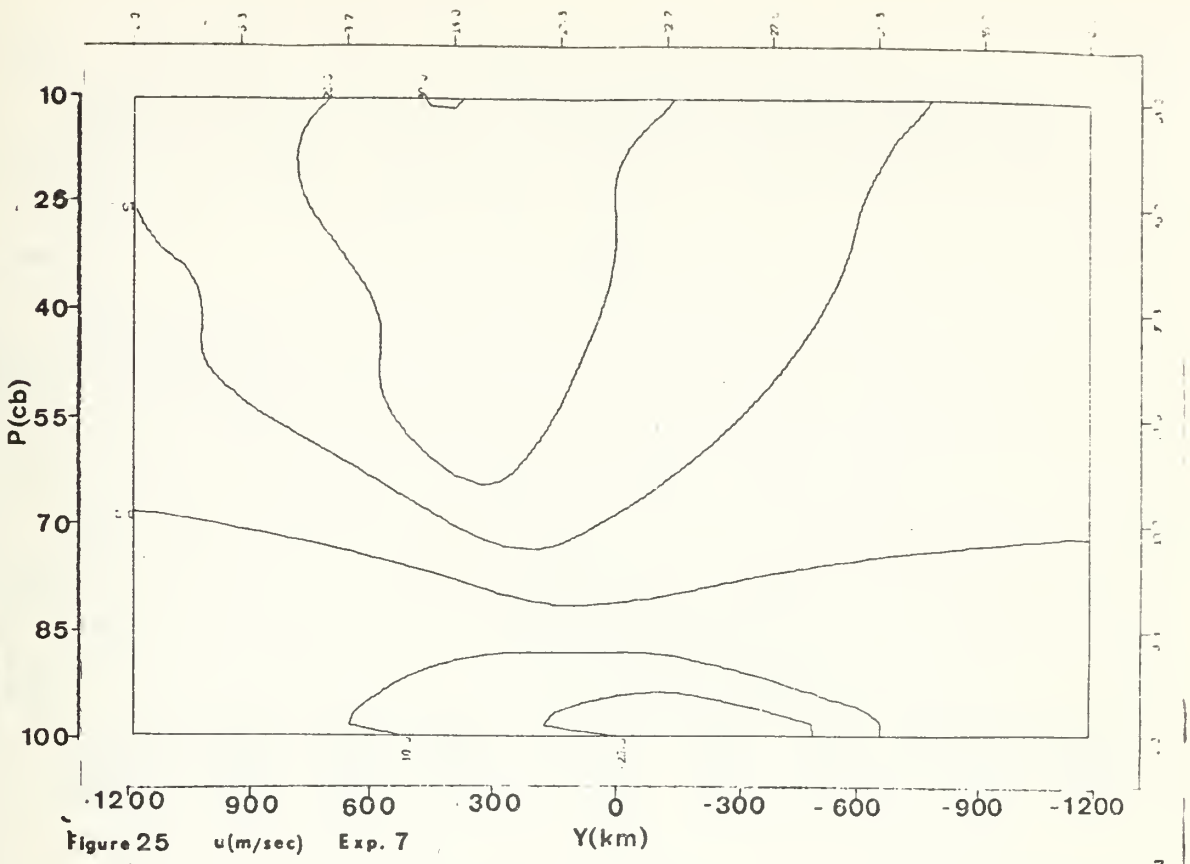

Figure 25 u(m/sec) Exp. 7

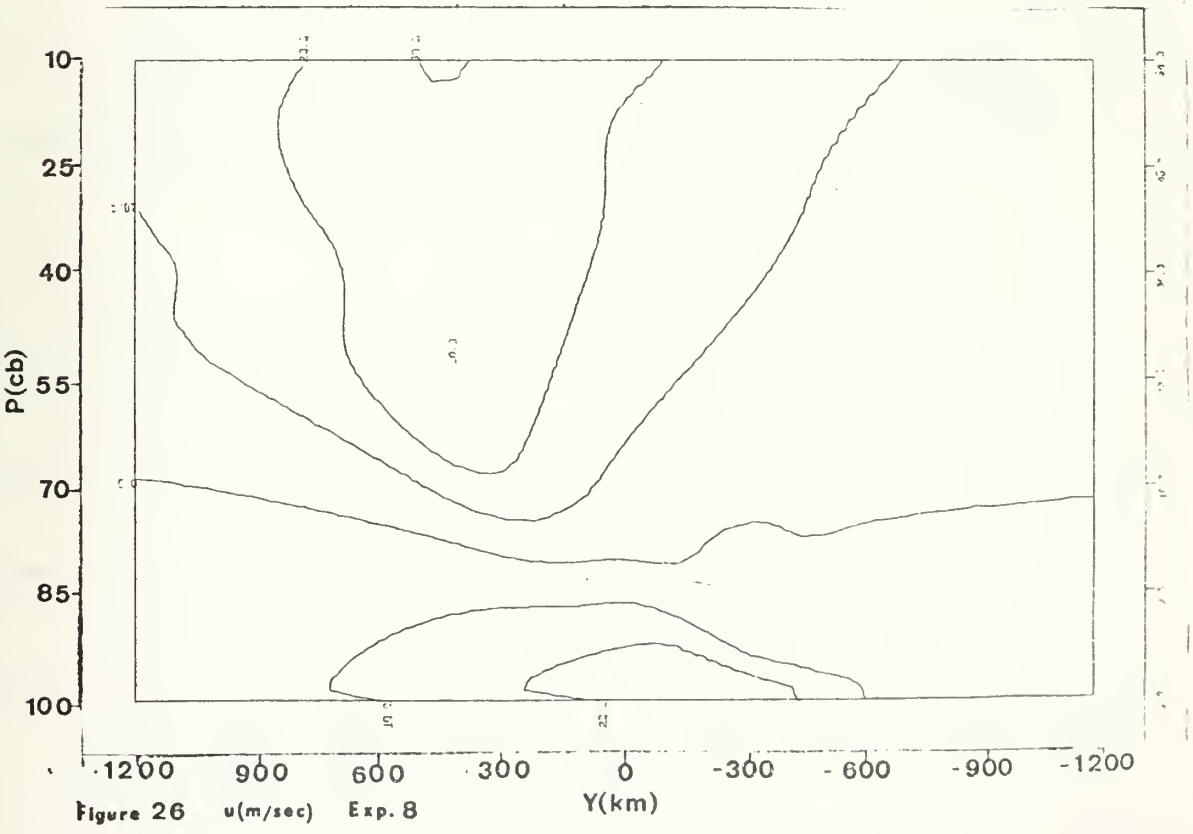

Figure 26 u(m/sec) Exp. 8

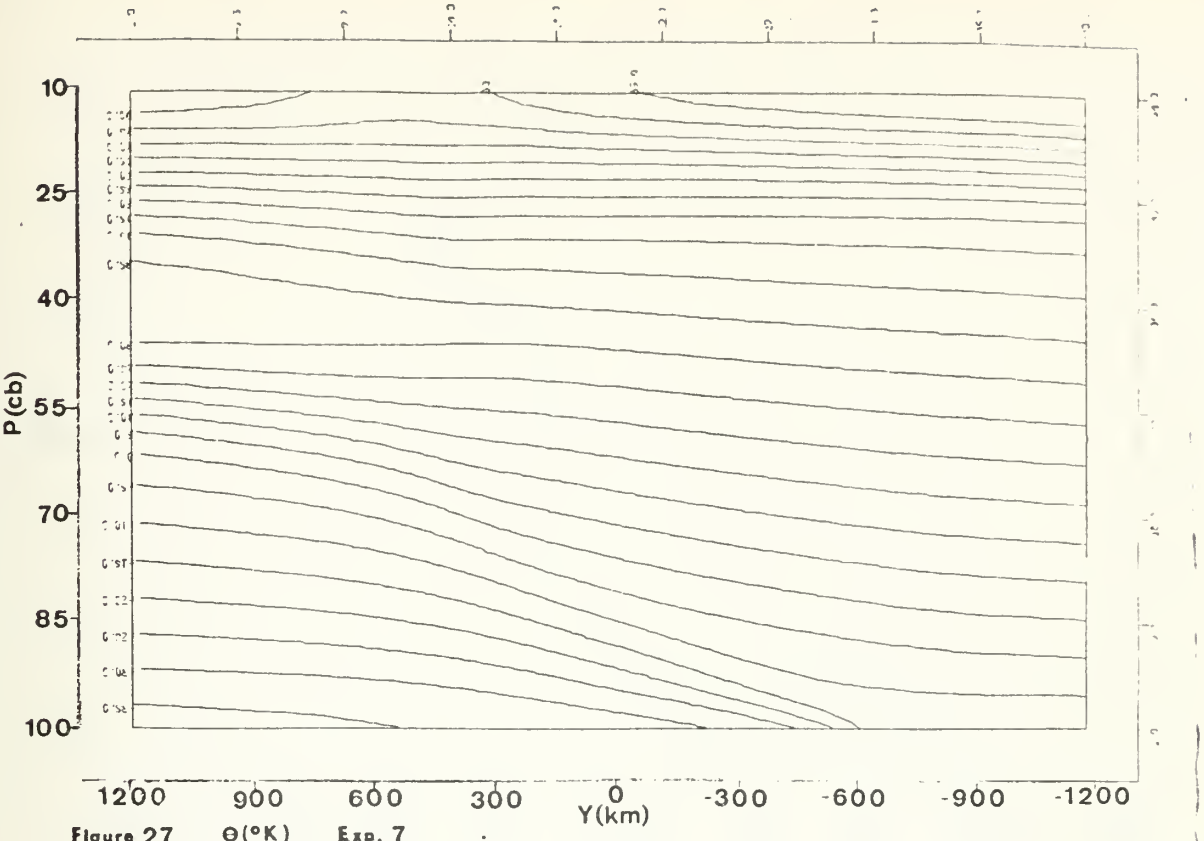

Figure 27 Θ(°K) Exp. 7

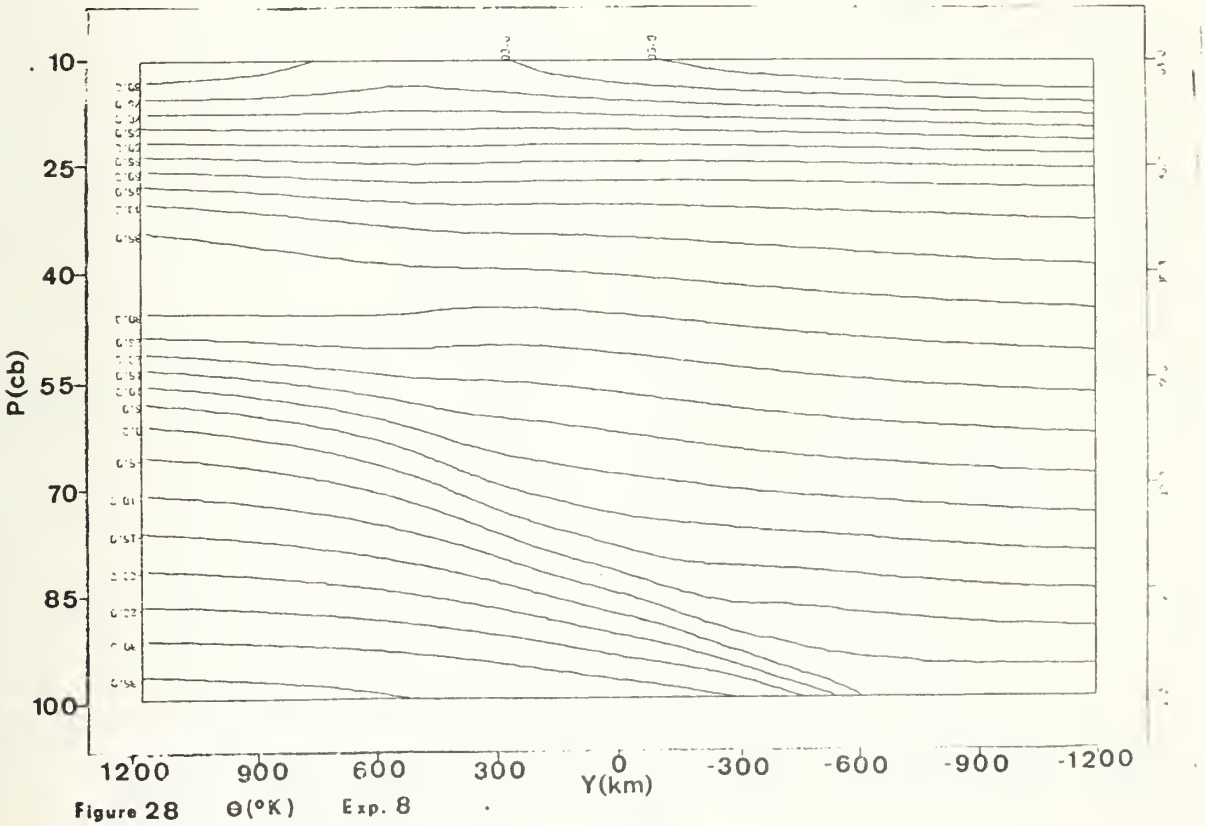

Figure 28 Θ(°K) Exp. 8

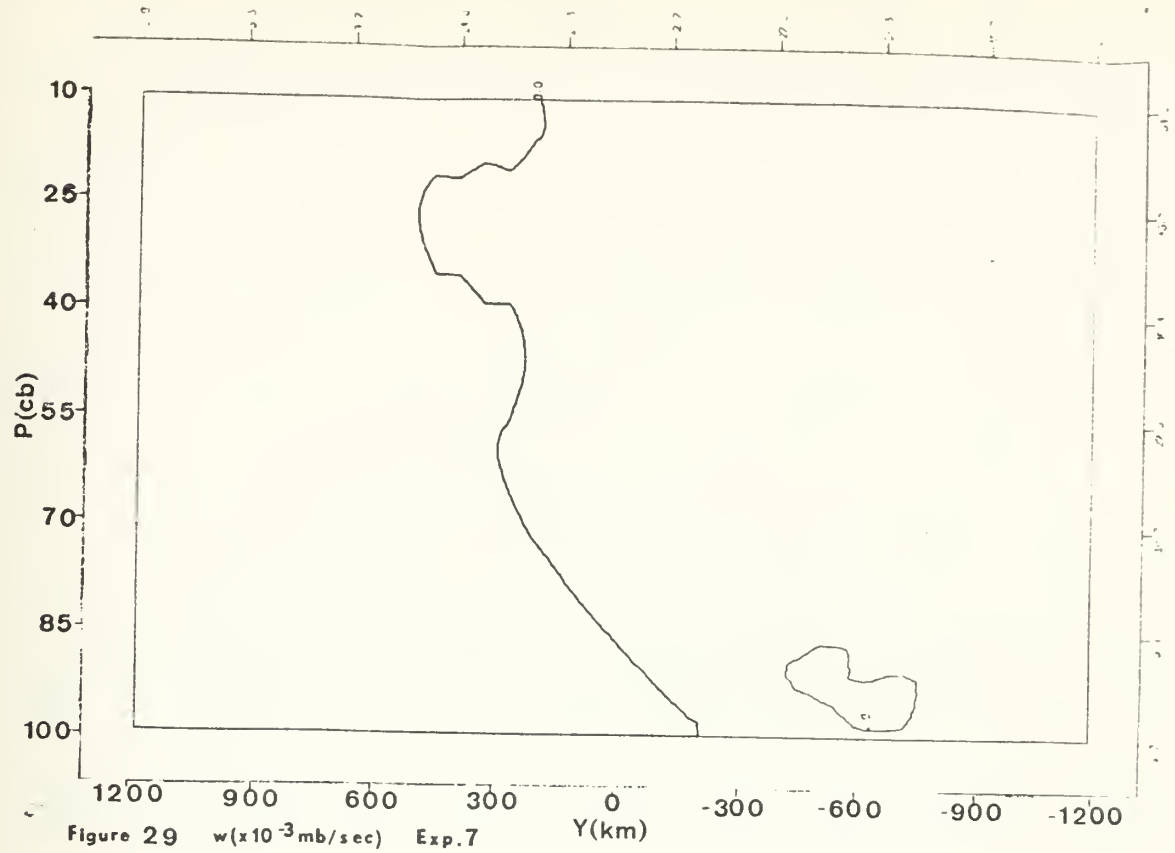

Figure 29 w(x10 $^{-3}$mb/sec) Exp.7

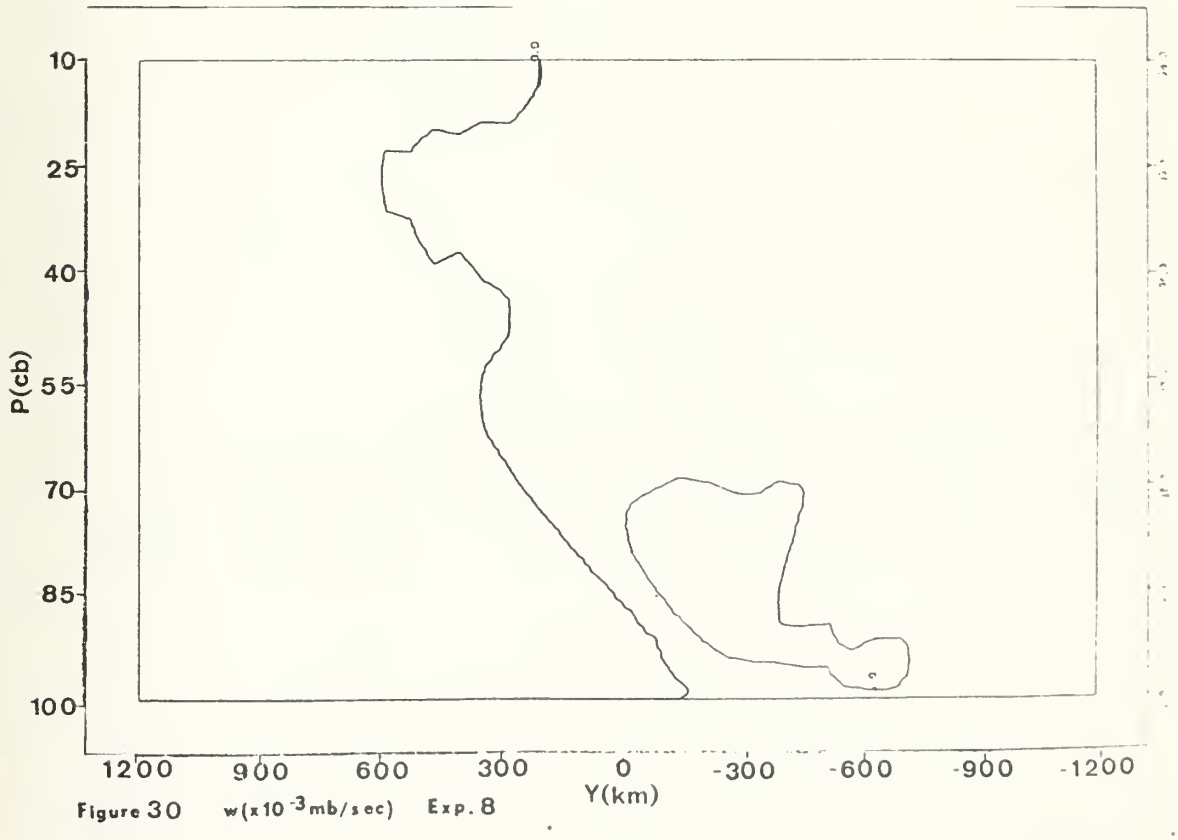

Figure 30 w(x10 $^{-3}$mb/sec) Exp. 8

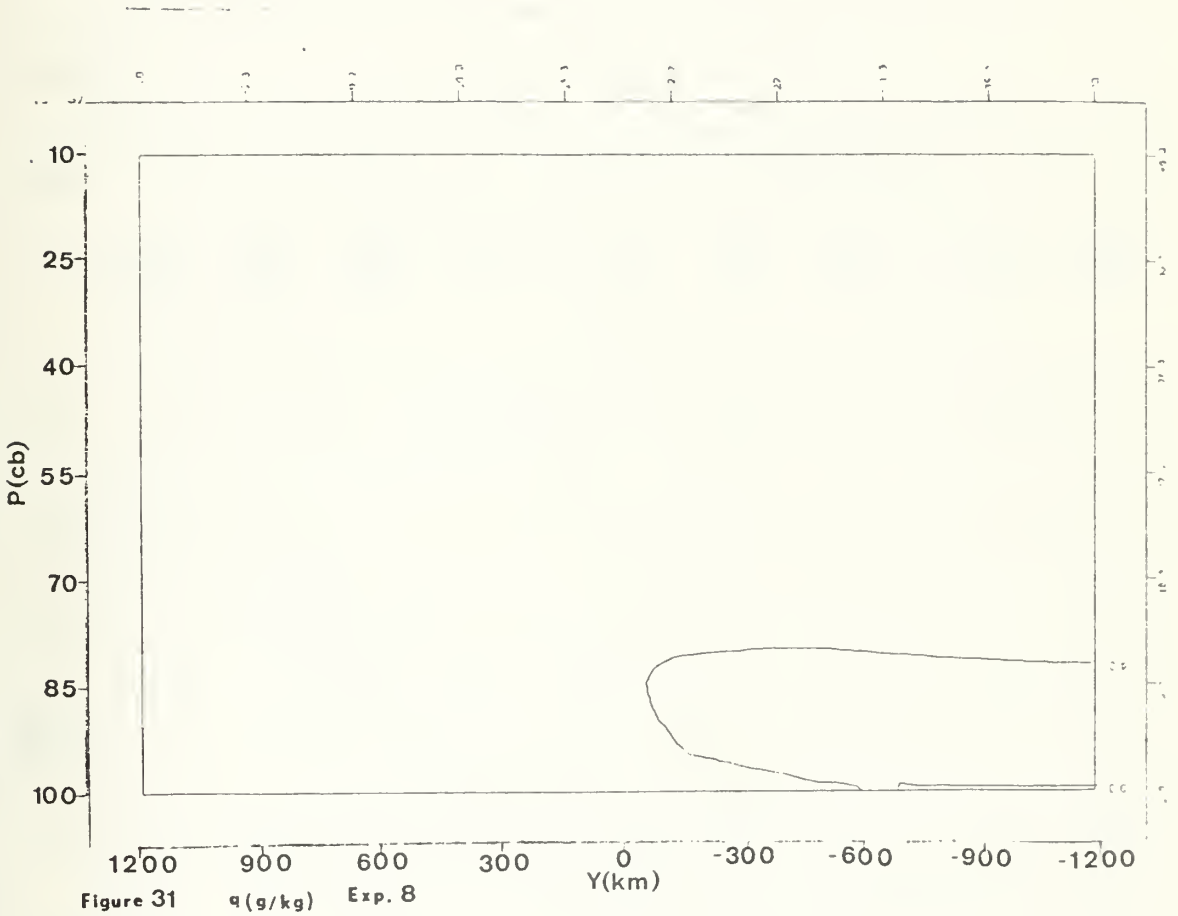

Figure 31 q(g/kg) Exp. 8

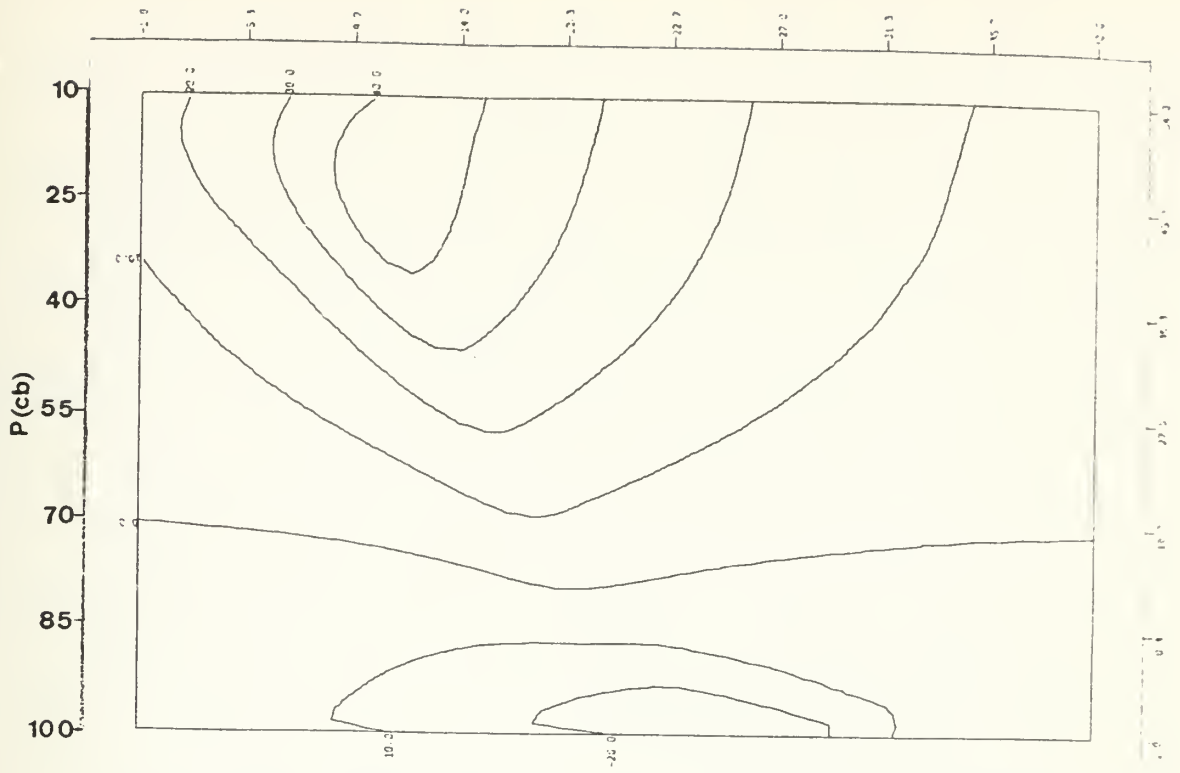

Figure 32 u(m/sec) Exp.9

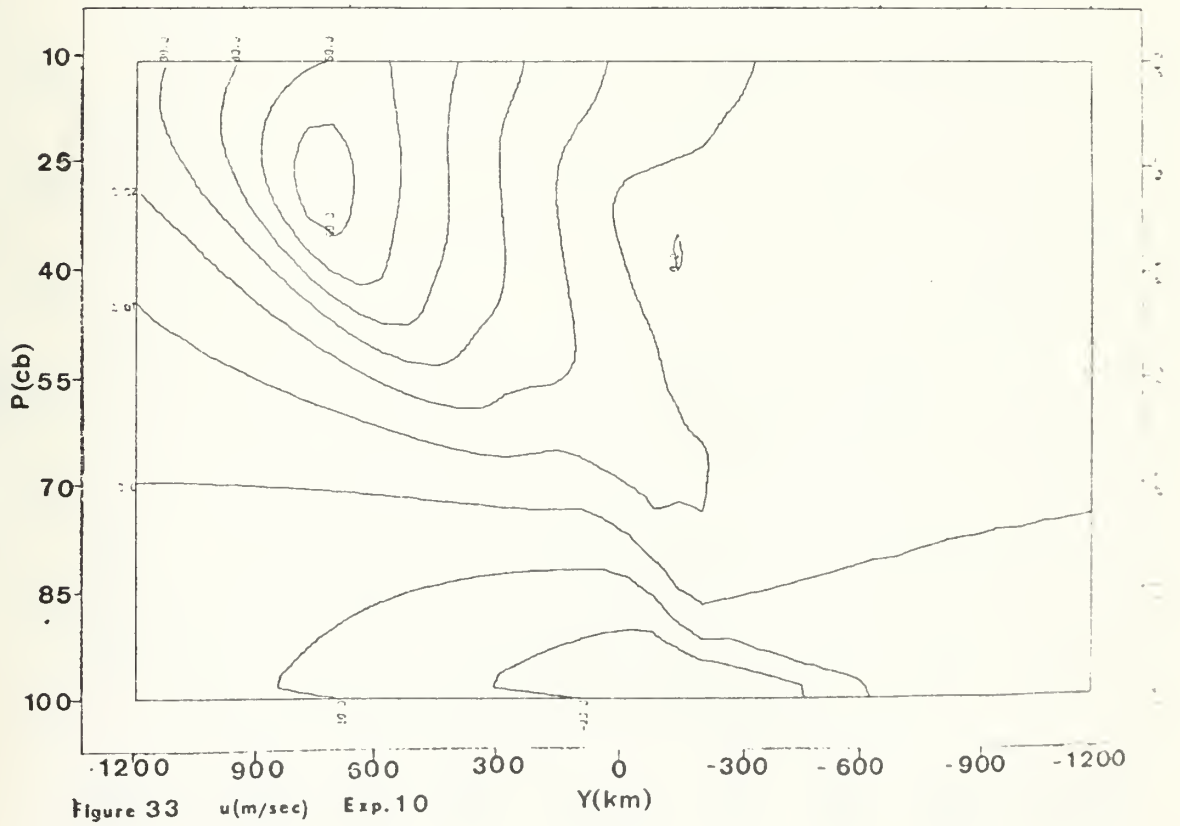

Figure 33 u(m/sec) Exp.10

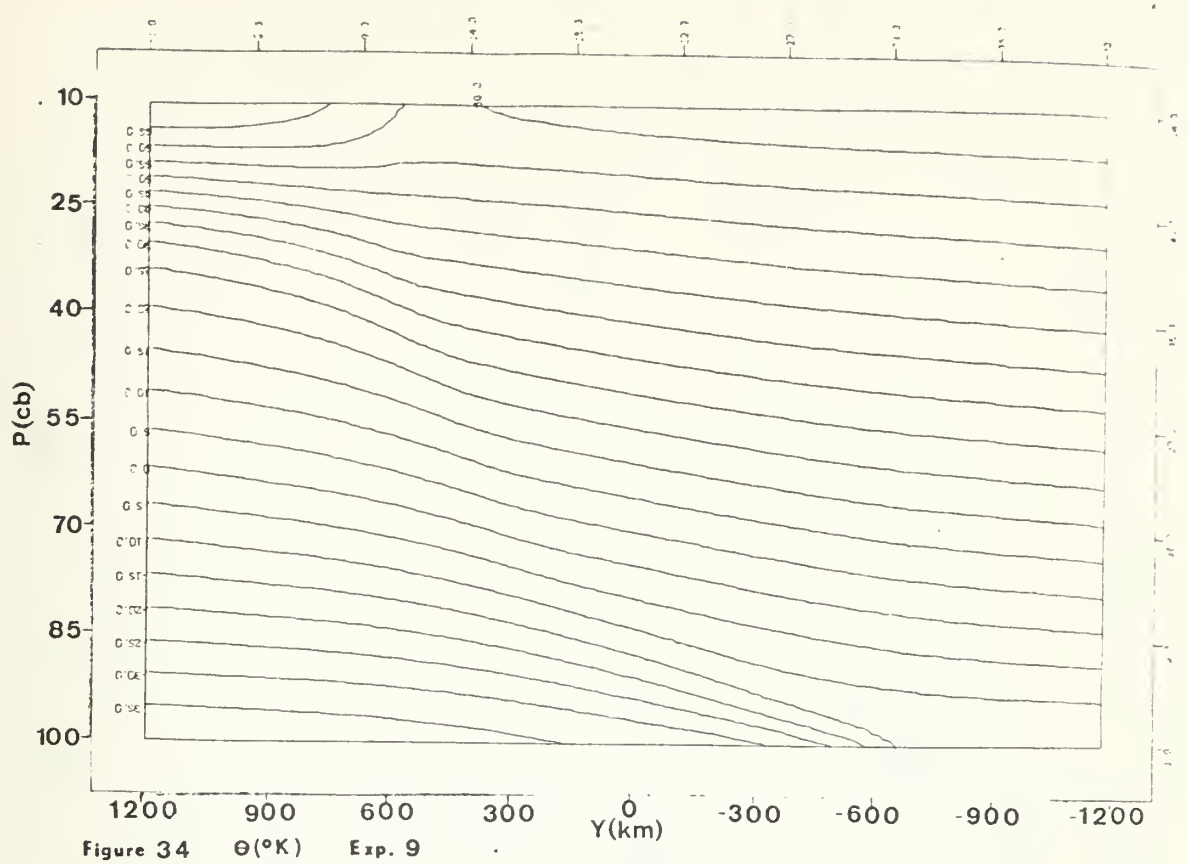

Figure 34 Θ(°K) Exp. 9

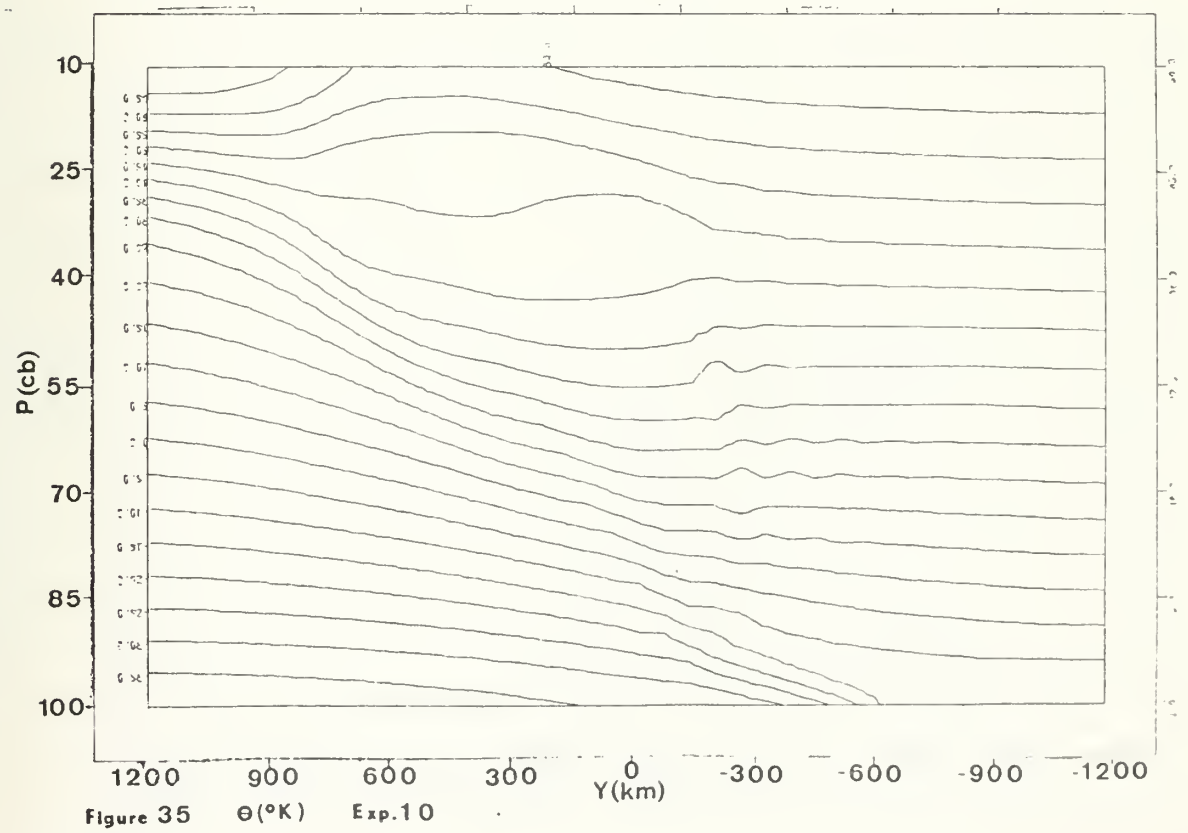

Figure 35 Θ(°K) Exp.10

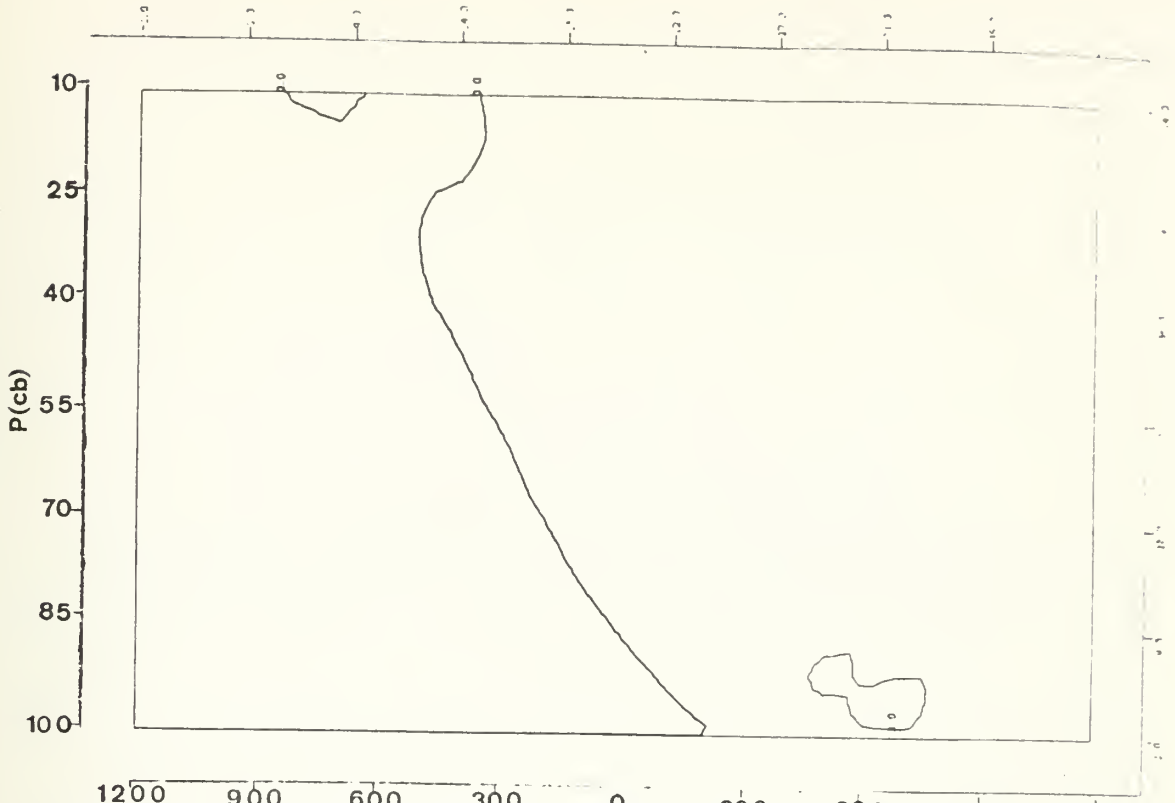

Figure 36 w(x10 $^{-3}$mb/sec) Exp. 9

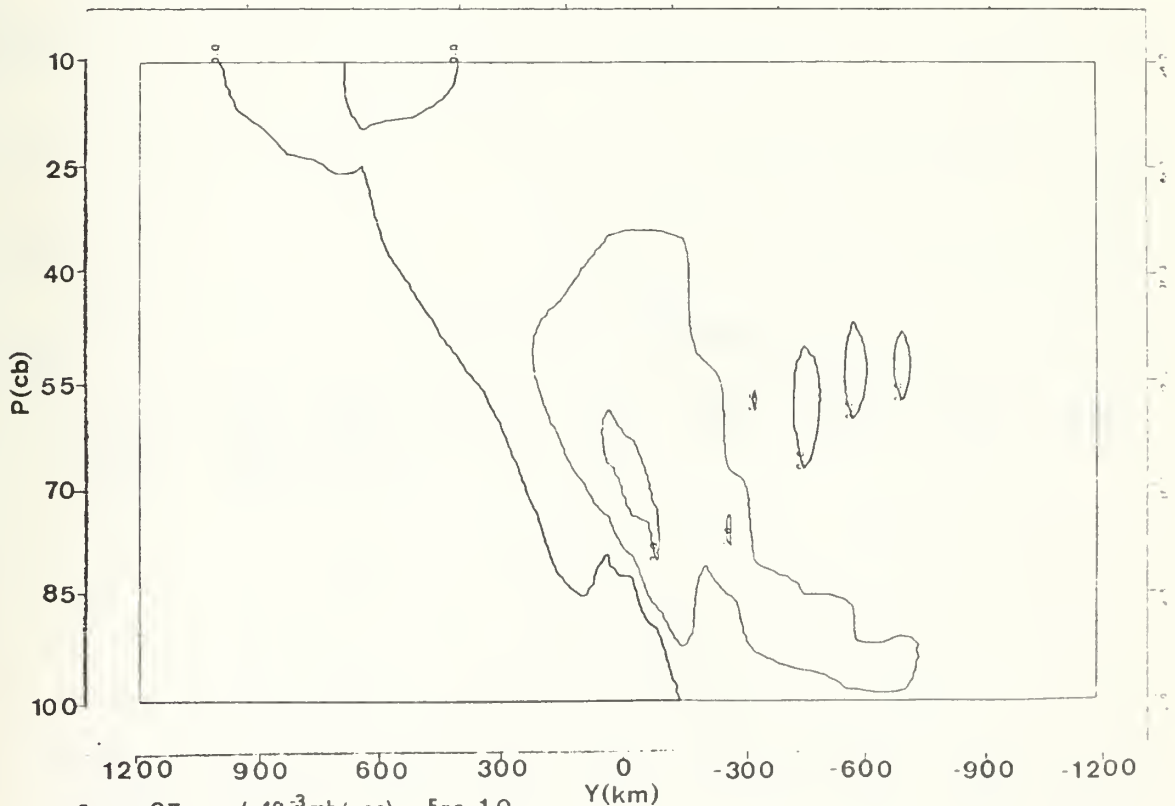

Figure 37 w(x10 $^{-3}$mb/sec) Exp.10

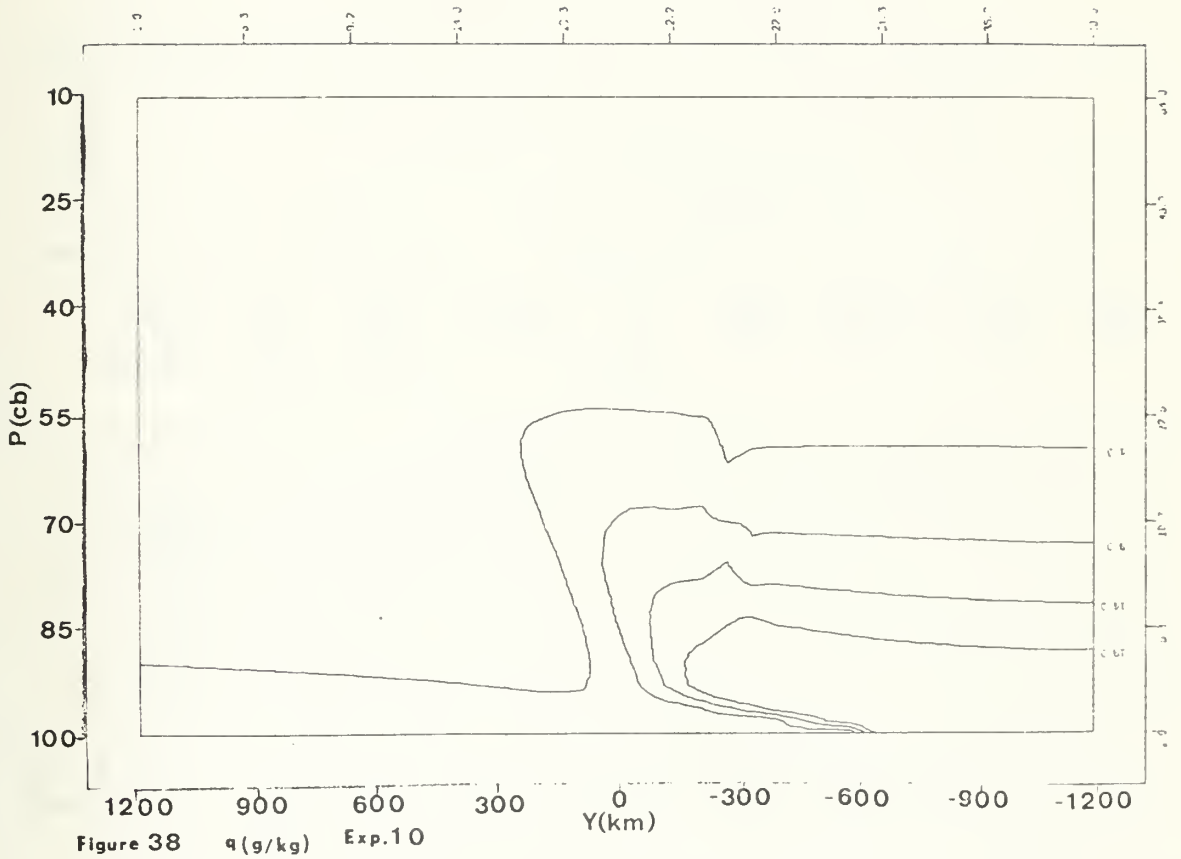

Figure 38 q(g/kg) Exp.10

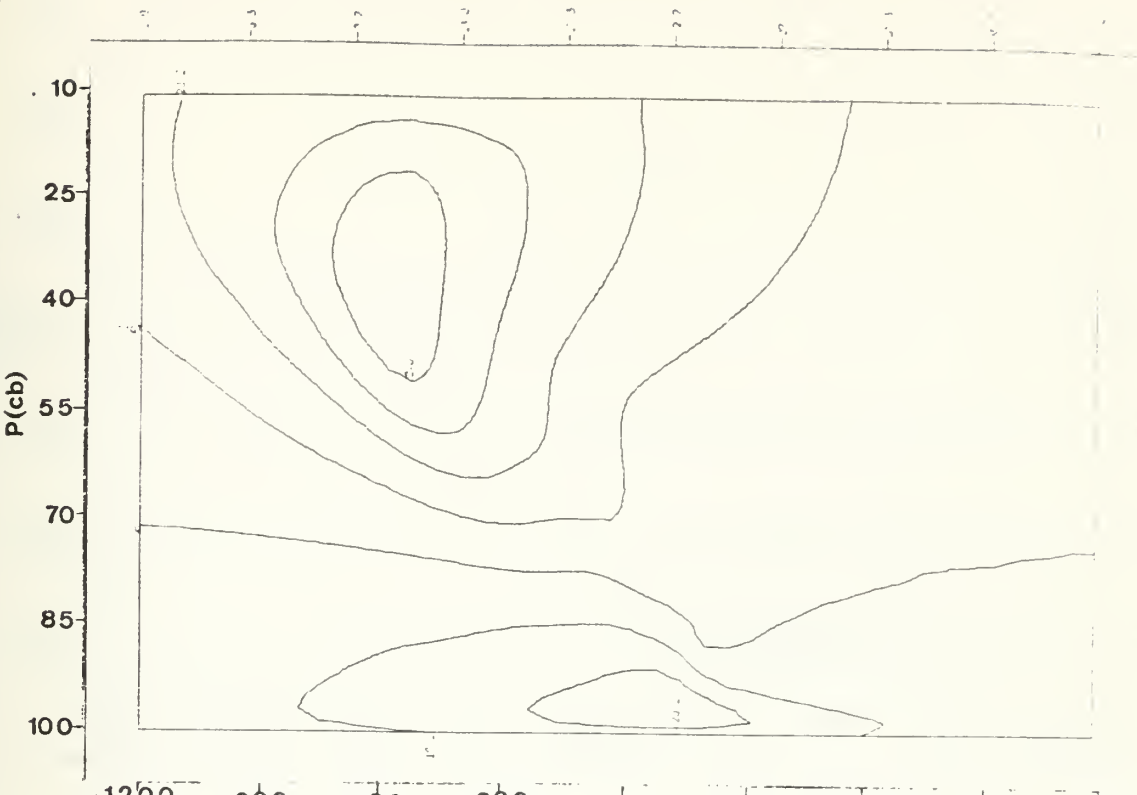

Figure 39 u(m/sec) Exp.11

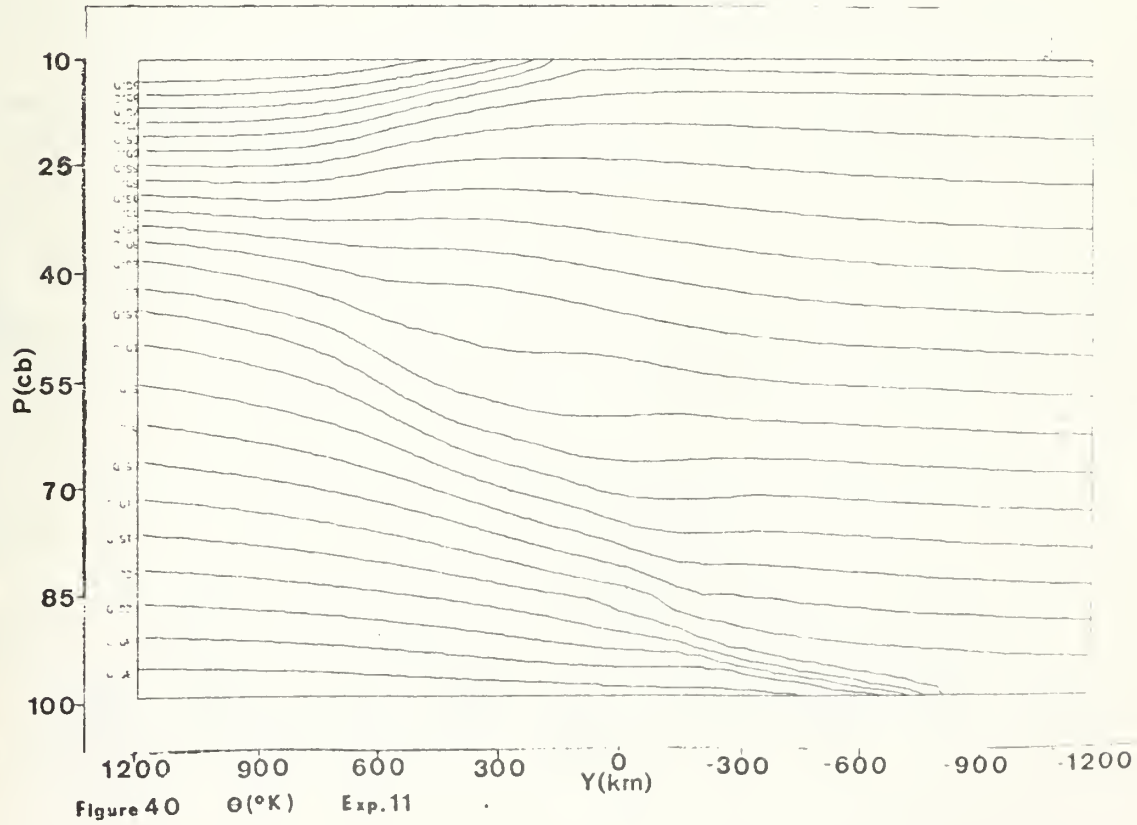

Figure 40 θ(°K) Exp.11

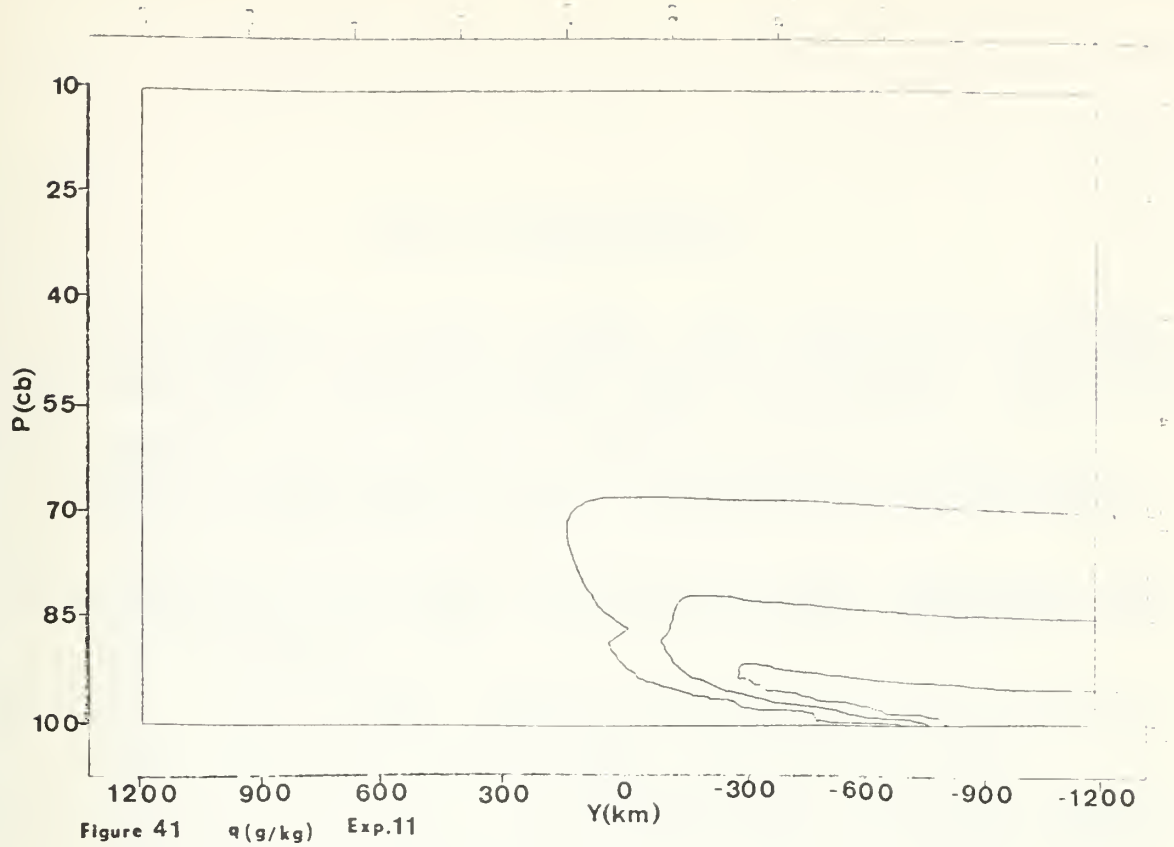

Figure 41 q(g/kg) Exp.11

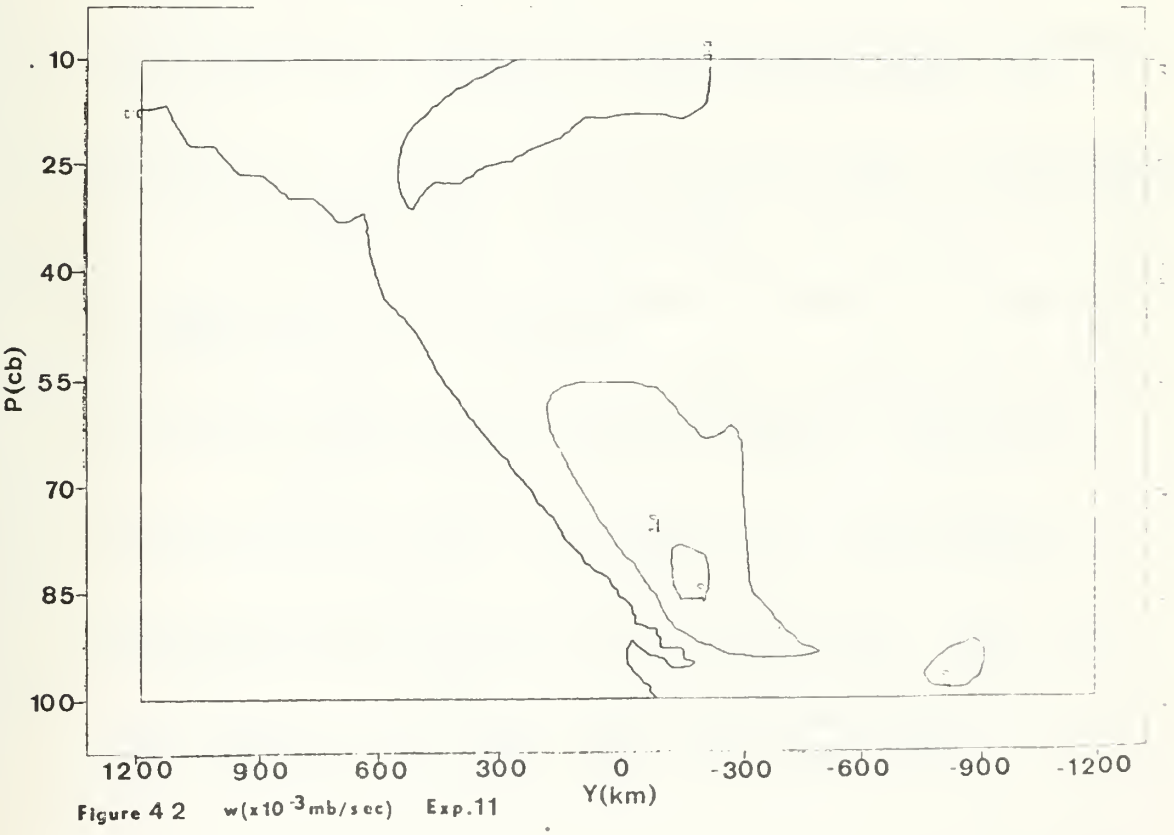

Figure 42 w(x10 $^{-3}$mb/sec) Exp.11

LIST OF REFERENCES

1. Cornelius, C. J., Jr., 1974: "The Inclusion of Moisture in a Numerical Model of Steady State Fronts". MS Thesis, Department of Meteorology, Naval Postgraduate School, 80 pp.

2. Haltiner, G. J., 1971: Numerical Weather Prediction Notes. Unpublished notes. Department of Meteorology, Naval Postgraduate School.

3. Haltiner, G. J., and F. L. Martin, 1957: Dynamical and Physical Meteorology, McGraw Hill Book Company, New York, 470 pp.

4. Hess, S. L., 1959: Introduction to Theoretical Meteorology, Henry Holt and Company, New York, 362 pp.

5. Holton, J. R., 1972: An Introduction to Dynamic Meteorology, International Geophysical series, Academic Press, New York, 16, 319 pp.

6. Hoskins, B. J., 1971: "Atmospheric Frontogenesis Models: Some Solutions." Quart. J. Roy. Meteor. Soc., 97, 139-153.

7. Hoskins, B. J., and F. P. Bretherton, 1972: "Atmospheric Frontogenesis Models: Mathematical Formulation and Solution." J. Atmos. Sci., 29, 11-37.

8. Mudrick, S. E., 1974: "A Numerical Study of Frontogenesis." J. Atmos. Sci., 31, 869-892.

9. Ogura, Y., and J. G. Charney, 1962: "A Numerical Model of Thermal Convection in the Atmosphere." Proc. Int. Symp. on Numer. Weather Predict., Tokyo, 431-452.

10. Williams, R. T., 1967: "Atmospheric Frontogenesis: A Numerical Experiment." J. Atmos. Sci., 24, 627-641.

11. _____ 1972: "Quasi-Geostrophic versus Non-geostrophic Frontogenesis." J. Atmos. Sci., 29, 3-10.

12. _____ 1974: "Numerical Simulation of Steady-State Fronts." J. Atmos. Sci., 31, 1286-1296.

INITIAL DISTRIBUTION LIST

		No. Copies
1.	Defense Documentation Center Cameron Station Alexandria, Virginia 22314	2
2.	Library, Code 0212 Naval Postgraduate School Monterey, California 93940	2
3.	Dr. R. T. Williams, Code 51 Wu Department of Meteorology Naval Postgraduate School Monterey, California 93940	2
4.	LCDR Daniel F. Glevy, Code 2200 Naval Electronics Laboratory Center Point Loma San Diego, California 92152	2
5.	Dr. G. Haltiner, Chairman, Code 51Ha Department of Meteorology Naval Postgraduate School Monterey, California 93940	1
6.	Dr. R. J. Renard, Code 51Rd Department of Meteorology Naval Postgraduate School Monterey, California 93940	1

160614

Glevy
The inclusion of vertical turbulent diffusion, moisture and a tropopause in a numerical model of steady state fronts.